

1 Introduction

With the advent of very energetic hadronic colliders like LHC and SSC, whose aim is to have access to the mechanism of electroweak symmetry breaking, a precise estimate of inclusive production of neutral clusters is mandatory to pin down signals due to Higgs particle or new physics [1]. Perturbative QCD is the appropriate framework to perform such a calculation provided large transfer momenta are involved. For this purpose leading order (hereafter denoted as LO) predictions - based on evaluations of partonic cross sections at tree level and evolution of structure and fragmentation functions at one loop level - are too rough. A consistent calculation at next to leading order (hereafter denoted as NLO) needs a NLO evaluation of parton-parton subprocesses which has been performed by our group [2] a few years ago utilizing existing results on the $O(\alpha_s^3)$ matrix element [3] and two loop evolved structure and fragmentation functions. Various sets of structure functions based on a NLO analysis using deep inelastic lepton nucleon scattering data, Drell-Yan production and direct photon production at hadronic accelerators are available in the literature [4, 5, 6].

Up to now such an analysis has not been performed for pions fragmentation functions since the only available derivation at NLO has been done for heavy quarks [7]. The parametrizations presently available [8] are based on a LO analysis of rather old e^+e^- data and semi inclusive deep inelastic muon nucleon scattering. Our aim is to perform a complete NLO evaluation of neutral pions inclusive production from hadronic colliders in order to estimate, as precisely as possible, the π^0 rates at LHC and SSC. The first step will consist in performing an extraction of pions fragmentation functions at NLO using e^+e^- data and hadronic data on one particle inclusive production. This will be done using three different methods. The first one, which does not exactly correspond to a NLO analysis but rather to an improved LO approximation, is based on the Monte-Carlo simulator HERWIG [9], whereas the second and the third ones are obtained from a two loop evaluation of evolution kernels previously computed [10, 11] together with NLO calculation of one hadron inclusive production from e^+e^- [12] and hadronic colliders [2] using respectively natural and optimized scales. As we will see it is not possible to extract an unique set of fragmentation functions which fits e^+e^- data around $\sqrt{S} = 30$ GeV [14, 15, 16, 17, 18] and hadronic data from fixed target domain [19, 20] to collider range [21, 22, 23]. We will therefore take different sets corresponding to different hypotheses on input fragmentation functions.

The paper is organized as follows. We recall the expressions of one particle inclusive production from e^+e^- and hadronic collisions and also give the evolution equations for fragmentation functions in section 2. Then in section 3 we discuss the extraction of various sets of fragmentation functions, first from HERWIG simulation and after through an exact NLO derivation. Predictions at LHC using the different sets previously obtained are displayed in section 4 together with a discussion of the resulting theoretical uncertainty. We give our

conclusions in section 5.

2 One particle inclusive production at next-to-leading order

Let us consider the inclusive production of a hadron H via the generic reaction $A + B \rightarrow H$ where A and B stand for hadrons and/or leptons. The cross-section can be written as a convolution of the fragmentation functions $D_l^H(z, M_f^2)$ with the partonic cross-section:

$$E_H \frac{d\sigma_{A+B \rightarrow H}}{d^3\vec{P}_H} = \sum_l \int_{z_H}^1 \frac{dz}{z^2} D_l^H(z, M_f^2) E_l \frac{d\sigma_{A+B \rightarrow l}}{d^3\vec{P}_l} \left(\frac{z_H}{z}, \theta, \alpha_s(\mu^2), M_f^2, \dots \right), \quad (1)$$

where z_H is the reduced energy of the hadron H : $z_H = 2E_H/\sqrt{S}$ and θ is the scattered angle of the parton l . The inclusive production of the parton l via the reaction $A + B \rightarrow l$ has the following perturbative development:

$$E_l \frac{d\sigma_{A+B \rightarrow l}}{d^3\vec{P}_l} \left(\frac{z_H}{z}, \theta, \alpha_s(\mu^2), M_f^2, \dots \right) = \sigma_{A+B \rightarrow l}^0 \left(\frac{z_H}{z}, \theta \right) + \frac{\alpha_s(\mu^2)}{2\pi} \sigma_{A+B \rightarrow l}^1 \left(\frac{z_H}{z}, \theta, M_f^2 \right) + \dots \quad (2)$$

Finally $D_l^H(z, M_f^2)$ represents the number of hadrons H inside the parton l carrying the fraction of impulsion z from H , evolved at the scale M_f^2 . These fragmentation functions satisfy Altarelli-Parisi type evolution equations:

$$\begin{aligned} \frac{\partial D_q^H(z, M_f^2)}{\partial \ln(M_f^2)} &= \frac{\alpha_s(M_f^2)}{2\pi} \int_z^1 \frac{dy}{y} \left[P_{qq}^T(y, \alpha_s(M_f^2)) D_q^H \left(\frac{z}{y}, M_f^2 \right) \right. \\ &\quad \left. + P_{gq}^T(y, \alpha_s(M_f^2)) D_g^H \left(\frac{z}{y}, M_f^2 \right) \right] \end{aligned} \quad (3)$$

$$\begin{aligned} \frac{\partial D_g^H(z, M_f^2)}{\partial \ln(M_f^2)} &= \frac{\alpha_s(M_f^2)}{2\pi} \int_z^1 \frac{dy}{y} \left[P_{gq}^T(y, \alpha_s(M_f^2)) D_q^H \left(\frac{z}{y}, M_f^2 \right) \right. \\ &\quad \left. + P_{gg}^T(y, \alpha_s(M_f^2)) D_g^H \left(\frac{z}{y}, M_f^2 \right) \right]. \end{aligned} \quad (4)$$

The evolution kernels have the perturbative development:

$$P_{ij}^T(x, \alpha_s(M_f^2)) = P_{ij}^0(x) + \frac{\alpha_s(M_f^2)}{2\pi} P_{ij}^{T1}(x) + \dots$$

In the following, we will drop the superscript index T. The Altarelli-Parisi kernels have been computed up to two loops order by Curci, Furmanski and Petronzio [11]. In the LO approximation one keeps only the first order in the perturbative development of the partonic cross-section and in the evolution kernels whereas at NLO one keeps the first and second terms in the perturbative expansion for both partonic cross-section and evolution kernels. We can split these fragmentation functions into a non-singlet and a singlet part:

$$D_i^-(z, M_f^2) \equiv \frac{1}{2} \left(D_{q_i}^H(z, M_f^2) - D_{\bar{q}_i}^H(z, M_f^2) \right) \quad (5)$$

$$D_i^+(z, M_f^2) \equiv \frac{1}{2} \left(D_{q_i}^H(z, M_f^2) + D_{\bar{q}_i}^H(z, M_f^2) \right) - \frac{1}{2N_f} D_S(z, M_f^2) \quad (6)$$

$$D_S(z, M_f^2) \equiv \sum_{i=1}^{N_f} \left(D_{q_i}^H(z, M_f^2) + D_{\bar{q}_i}^H(z, M_f^2) \right). \quad (7)$$

In the evolution equations the singlet part D_S is coupled to the gluon fragmentation function whereas the non-singlet parts D^- and D^+ are decoupled. Note a misprint in ref. [11] and the correspondence with our notation:

$$\begin{aligned} P_{gg}^i &= P_{GG} \\ P_{qg}^i &= P_{GF}/(2N_f) \\ P_{gq}^i &= 2N_f P_{FG} \\ P_{qq}^i &= P_{FF}. \end{aligned}$$

Once input fragmentation functions have been specified at some reference scale M_{f0} the evolution equations are solved using an inverse Mellin transform technique. Let us consider now in detail the partonic cross-sections.

2.1 $e^+e^- \rightarrow \pi^0$

The partonic cross sections from e^+e^- collisions read at next-to-leading order:

$$\begin{aligned} E_{q_i} \frac{d\sigma_{e^+e^- \rightarrow q_i}}{d^3\vec{P}_{q_i}}(y, \theta, \alpha_s(\mu^2), M_f^2) = \\ \frac{6\sigma_0}{\pi Q^2 y} e_i^2 \left\{ \frac{3}{8}(1 + \cos^2\theta) \left[\delta(1-y) + \frac{\alpha_s(\mu^2)}{2\pi} \left(P_{qq}^0(y) \ln\left(\frac{Q^2}{M_f^2}\right) + K_q^T(y) \right) \right] \right. \\ \left. + \frac{3}{4}(1 - \cos^2\theta) \frac{\alpha_s(\mu^2)}{2\pi} K_q^L(y) \right\} \quad (8) \end{aligned}$$

$$\begin{aligned} E_g \frac{d\sigma_{e^+e^- \rightarrow g}}{d^3\vec{P}_g}(y, \theta, \alpha_s(\mu^2), M_f^2) = \\ \frac{12\sigma_0}{\pi Q^2 y} \sum_{i=u,d,s,c,\dots} e_i^2 \left\{ \frac{3}{8}(1 + \cos^2\theta) \left[\frac{\alpha_s(\mu^2)}{2\pi} \left(P_{gq}^0(y) \ln\left(\frac{Q^2}{M_f^2}\right) + K_g^T(y) \right) \right] \right. \\ \left. + \frac{3}{4}(1 - \cos^2\theta) \frac{\alpha_s(\mu^2)}{2\pi} K_g^L(y) \right\}, \quad (9) \end{aligned}$$

where σ_0 is the usual point like cross-section

$$\sigma_0 = \frac{4\pi\alpha^2}{3Q^2},$$

α is the QED coupling constant and Q^2 is the invariant mass of the e^+e^- pair. The functions K_q^T , K_q^L , K_g^T and K_g^L have been extracted from the reference [12] (see also [13]).

$$K_q^T(x) = C_F \left\{ \frac{3}{2}(1-x) - \frac{3}{2} \frac{1}{(1-x)_+} + 2 \frac{1+x^2}{1-x} \ln(x) \right\}$$

$$+ (1+x^2) \left(\frac{\ln(1-x)}{1-x} \right)_+ + \left(\frac{2\pi^2}{3} - \frac{9}{2} \right) \delta(1-x) \Big\}, \quad (10)$$

$$K_g^T(x) = C_F \left\{ \frac{1+(1-x)^2}{x} (\ln(1-x) + 2\ln(x)) - 2\frac{1-x}{x} \right\} \quad (11)$$

$$K_q^L(x) = C_F \quad (12)$$

$$K_g^L(x) = 2 C_F \frac{1-x}{x}. \quad (13)$$

In the above equations two scales are involved: the renormalization scale μ at which the running coupling constant α_s is evaluated and the fragmentation scale M_f at which fragmentation functions are evolved. The choice for these scales is rather arbitrary. Note that for every y , $K_g^T(y)$ is negative, so the choice $M_f^2 = Q^2$ leads to a negative contribution to the partonic cross-section $E_g d\sigma_{e^+e^- \rightarrow g} / d^3\vec{P}_g$.

The running coupling of QCD α_s is defined at the next-to-leading logarithm approximation by the approximate analytical formula:

$$\alpha_s(\mu^2) = \frac{1}{b \ln(\mu^2/\Lambda^2)} \left[1 - \frac{b'}{b} \frac{\ln \ln(\mu^2/\Lambda^2)}{\ln(\mu^2/\Lambda^2)} \right]. \quad (14)$$

In section 3 we will also use for α_s the numerical solution of the equation:

$$\frac{1}{\alpha_s(\mu^2)} + b' \ln \left(\frac{b' \alpha_s(\mu^2)}{1 + b' \alpha_s(\mu^2)} \right) = b \ln \left(\frac{\mu^2}{\Lambda^2} \right), \quad (15)$$

with:

$$b = \frac{33 - 2N_f}{12\pi}, \quad b' = \frac{153 - 19N_f}{24\pi^2},$$

which is more appropriate than eq.(14) for small scales μ . Indeed for large μ the two definitions agree but for small μ they can differ by more than 20 %.

2.2 $p p \rightarrow \pi^0$

The partonic cross-sections for hadronic collisions are given by [2]:

$$E_l \frac{d\sigma_{p+p \rightarrow l}}{d^3\vec{P}_l}(y, \theta, \alpha_s(\mu^2), M_f^2) = \frac{1}{\pi S} \sum_{i,j} \int_{VW}^V \frac{dv}{1-v} \int_{VW/v}^1 \frac{dw}{w} \\ \times \left[F_i^p(x_1, M^2) F_j^p(x_2, M^2) \left(\frac{1}{v} \left(\frac{d\sigma^0}{dv} \right)_{ij \rightarrow l}(s, v) \delta(1-w) \right. \right. \\ \left. \left. + \frac{\alpha_s(\mu^2)}{2\pi} K_{ij \rightarrow l}(s, v, w; \mu^2; M^2, M_f^2) \right) + (x_1 \leftrightarrow x_2) \right]. \quad (16)$$

The variables V, W are defined by

$$V = 1 - \frac{y}{2}(1 - \cos \theta), \quad W = \frac{y(1 + \cos \theta)}{2 - y(1 - \cos \theta)},$$

and we also have

$$x_1 = \frac{VW}{vw}, \quad x_2 = \frac{1-V}{1-v}$$

and $s = x_1 x_2 S$. At NLO sixteen subprocesses contribute to the cross-section. The terms σ^0 correspond to the lowest order $2 \rightarrow 2$ parton scattering subprocesses whereas the terms K contain the one loop corrections to these subprocesses. In the hadronic case, we have three scales: the renormalization scale μ , the factorization scale for the initial state M (the scale of the distribution functions) and the factorization scale for final state M_f (the scale of the fragmentation functions). Schematically, the hadronic cross-section can be written as:

$$E_{\pi^0} \frac{d\sigma_{p+p \rightarrow \pi^0}}{d^3 \vec{P}_{\pi^0}} = \alpha_s^2(\mu^2) A + \alpha_s^3(\mu^2) \left[2bA \ln\left(\frac{\mu^2}{\Lambda^2}\right) + B \ln\left(\frac{M^2}{\Lambda^2}\right) + C \ln\left(\frac{M_f^2}{\Lambda^2}\right) + D \right]. \quad (17)$$

We show explicitly the dependence of the hadronic cross-section upon the three scales μ , M and M_f . The four functions A, B, C and D depend on the scales M and M_f via the structure and fragmentation functions. In addition, A, B and C are scheme independent. We always use the \overline{MS} scheme for final factorization whereas the initial factorization scheme is fixed by the set of structure functions used.

Let us discuss now the partonic cross-sections. In order to determine the kinematical region where each partonic reaction dominates we have plotted in figures 1a, 1b, 1c and 1d the partonic cross-sections $E_l d\sigma_{p+p \rightarrow l} / d^3 \vec{P}_l$ for $l = g, u + \bar{u} + d + \bar{d}, s + \bar{s} + c + \bar{c}$ against P_t at the leading log level for various center of mass energies. We think it is meaningless to use next-to-leading formulae since the dependence on $\ln(M_f^2)$ is not balanced. We have used ABFOW structure functions [6]. We see that for the low center-of-mass energy experiments WA70 [19] ($\sqrt{S} = 23$ GeV) and E706 [20] ($\sqrt{S} = 31$ GeV) the gluon and the valence quarks contributions are of the same order at low P_{tl} , whereas when P_{tl} becomes larger, the valence quarks dominate. For ISR experiments [21],[22] ($\sqrt{S} = 63$ GeV) the glue contribution dominates up to $P_{tl} \simeq 10$ GeV. For the UA2 experiment [23], when the pseudo rapidity $\eta = 1.4$, the glue contribution is important up to $P_{tl} \simeq 35$ GeV. Finally for LHC, in the P_{tl} range between 30 and 1000 GeV the glue contribution represents (60 - 80) % of the partonic cross-section. In all cases the "sea" contribution (s,c) is always negligible.

In order to estimate the z range we are sensitive to we will study in table I the integrand of eq. (1), i.e.:

$$\langle z \rangle = \frac{\int \frac{dz}{z} \sum_l D_l^{\pi^0}(z, M_f^2) E_l \frac{d\sigma_{p+p \rightarrow l}}{d^3 \vec{P}_l}}{\int \frac{dz}{z^2} \sum_l D_l^{\pi^0}(z, M_f^2) E_l \frac{d\sigma_{p+p \rightarrow l}}{d^3 \vec{P}_l}} \quad (18)$$

with z varying between $2E_{\pi^0}/\sqrt{S}$ and 1. Note that the partonic cross-sections reach their maximum for $z = 1$ while the fragmentation functions decrease with z . As we can infer from Table I the large z region is kinematically favored. We have used set I of fragmentation functions which will be discussed later.

As already mentioned the fragmentation functions are known less accurately than the structure functions. Up to now they have been extracted at LO [8] from e^+e^- annihilation and semi inclusive deep inelastic muon nucleon scattering. No extraction from hadronic colliders data has been performed so far. In the following we will carry out an extraction of π^0 fragmentation functions at NLO accuracy, using three different approaches.

3 Extraction of π^0 fragmentation functions.

3.1 Selection of experimental data.

We first discuss the experimental data we will use to extract the π^0 fragmentation functions. We first consider e^+e^- collisions. The JADE collaboration [18] has published data at $\sqrt{S} = 14, 22.5$ and 34.4 GeV. We use the data at 34.4 GeV, covering mainly the low z_H range (up to $z_H = 0.209$). Data from the TPC collaboration [17] at $\sqrt{S} = 29$ GeV are given as $\frac{1}{\sigma_{had}} \frac{d\sigma}{\beta dz_H}$, therefore a value of $R=4.00$ is assumed to bring them to the usual form $\frac{S}{\beta} \frac{d\sigma}{dz_H}$. Data from the TASSO collaboration [16] at $\sqrt{S} = 34.6$ GeV extend up to $z_H = 0.728$. The broadest z_H range is covered by data from the CELLO collaboration, extending from $z_H = 0.049$ to $z_H = 0.919$ at $\sqrt{S} = 35$ GeV [15] and from $z_H = 0.094$ to $z_H = 0.847$ at $\sqrt{S} = 22$ GeV [14]. Data from experiments at DORIS are not used, as hardly any point survive with the cut on the lower energy of the π^0 at 2 GeV. Data obtained at LEP are for the moment not constraining. However, cross checks have been performed with the 2 points surviving the cut of data from the Argus collaboration [25] at $\sqrt{S} = 10$ GeV and the 4 points from the L3 collaboration [26] at $\sqrt{S} = 91$ GeV.

Let us discuss now experimental data from hadronic colliders. Data in hadronic reactions have been selected for this study taking into account statistical and systematic accuracy. Whenever possible, reconstructed π^0 are preferred. For SPS fixed target energies, the available data in pp reactions are in reasonable agreement and we will use the data in the central rapidity range at $\sqrt{S} = 23$ GeV, from the WA70 collaboration [19]. The FNAL fixed target range overlaps with the lower ISR energy range. The recent data at $\sqrt{S} = 31$ GeV from pBe reactions obtained by the E706 collaboration [20] are in agreement with some of the ISR results. Resolved π^0 at $\sqrt{S} = 62.8$ GeV taken from table 5 (more precisely data corresponding to the super-retracted geometry) of Kourkoumelis et al. [22] are used. They will be compared with other data available at this energy. We will use also the more recent data from the AFS collaboration [21], which however show a different P_t dependence. At collider energies, the latest data from the UA2 experiment at $\sqrt{S} = 630$ GeV with average pseudo rapidity $\eta = 1.4$ will be used [23]. Cross checks have been made

with data at $\sqrt{S} = 540$ GeV with average pseudo rapidity $\eta = 0$ although π^0 are not disentangled from direct photons.

3.2 Fragmentation functions from HERWIG.

We first consider the π^0 inclusive production in e^+e^- annihilation at $M_{f0} = \sqrt{S} = 30$ GeV, as simulated by the Monte Carlo generator HERWIG. As well known, this event generator includes the QCD parton shower to leading and next to leading accuracy - in particular the kinematical corrections due to the phase space boundaries are summed up to all orders - as well as the hadronisation of the color singlet clusters into the physical particles. Furthermore HERWIG has been shown [24] to describe with good accuracy the observed features of PETRA and LEP data. Then we will use the π^0 distribution generated by each quark flavor which originates from the photonic vertex, as a realistic description of the quark fragmentation into π^0 . Owing to the symmetry of quarks and antiquarks fragmenting into π^0 we extract the quark fragmentation functions from:

$$\frac{d\sigma_{e^+e^- \rightarrow \pi^0}}{dz_H}(z_H, M_{f0}^2) \sim 6\sigma_0 \sum_q e_q^2 D_q^{\pi^0}(z_H, M_{f0}^2), \quad (19)$$

where the pointlike cross section σ_0 has been previously defined. The reaction $e^+e^- \rightarrow \pi^0 + X$ has been therefore decomposed into each contribution $e^+e^- \rightarrow u\bar{u}, d\bar{d}, s\bar{s}, c\bar{c}$ and $b\bar{b}$. The generated distributions are parametrized as

$$D_i^{\pi^0}(z, M_{f0}^2) = N_i z^{\alpha_i} (1-z)^{\beta_i} \quad (20)$$

and analyzed using the minimization procedure MINUIT. The coefficients N_i are constrained by the normalization condition:

$$\int_{\frac{2m_\pi}{M_{f0}}}^1 dz D_i(z, M_{f0}^2) = \langle n_\pi \rangle_i, \quad (21)$$

where the average values $\langle n_\pi \rangle_i$ are given by HERWIG for each quark flavor, in agreement with the total observed multiplicity $\langle n_\pi \rangle$. The parameters N_i, α_i and β_i are extracted from the π^0 inclusive distribution generated, for each flavor, in the x range $.025 \leq z_H \leq .95$ and shown in table II. As can be inferred from this table the statistical error on the parameters is less than 5%.

As an illustration of the accuracy of the method and also of its limitations, the π^0 inclusive cross-section obtained from eqs. (19) and (20), together with the results of table II, are compared in figure 2 with the CELLO data [15] at $\sqrt{S} = 35$ GeV. The agreement is reasonable in the range $z_H \leq .5$. So far we have not included the contribution from the gluon fragmentation function. Indeed from the analysis of the three jet events it would be possible, in principle, to extract from HERWIG the appropriate information. The corresponding accuracy is however unsatisfactory, due to the limited sensitivity to hard gluon effects in e^+e^- annihilation.

For this reason we have followed a different approach. To extract the gluon fragmentation function from HERWIG we have analyzed the subprocess $gg \rightarrow gg \rightarrow \pi^0 + X$ from $p\bar{p}$ annihilation at $M_{f0} = \sqrt{s} \sim 30$ GeV, in analogy to the quark case. In order to eliminate the background from the fragmentation of the spectator partons we have considered the pions lying only within a cone of semi aperture $\delta = .35 - .40$ rad around the direction of the parent gluons emitted at 90 deg. The value of δ is found by an appropriate angular study of the generated distribution. With a parametrization of the form (20) we find the values of the parameters N_g, α_g and β_g given in table III. After inclusion of the gluon fragmentation function and use of NLO evolved fragmentation functions together with NLO terms in the π^0 inclusive cross section the agreement with CELLO data is improved as can be inferred from figure 3 up to $z_H \simeq 0.8$

We compare now our predictions at NLO to experimental data from hadronic colliders. We first consider the data from CERN ISR [21, 22], for $\sqrt{S} = 63$ GeV, compared in figures 4 and 5 with our predictions for $\mu = M = M_f = P_t$ and $\mu = M = M_f = P_t/2$ using the quark fragmentation functions from table II and the two gluon sets from table III, with $\delta = 0.35$ and $\delta = 0.40$. The agreement is satisfactory within the theoretical and experimental uncertainties.

Let us focus now on the UA2 data at the $Spp\bar{p}S$ collider [23]. We will use two sets of quite precise data, for $P_t \leq 15$ GeV and $\eta \simeq 0$ and, for $15 \leq P_t \leq 45$ GeV and $\eta \simeq 1.4$. The comparison with the theoretical predictions is shown in figures 6 and 7 for $\mu = M = M_f = P_t/2$, P_t and for the two gluon sets of fragmentation functions. The agreement is quite good, and slightly favors the set corresponding to $\delta = 0.35$. The dependence on the renormalization, factorization and fragmentation scales at NLO will be discussed later.

In the next subsection we will extract the π^0 fragmentation functions at next to leading order using two different hypotheses at the reference scale $M_{f0}^2 = 2$ GeV².

3.3 Set I: fragmentation functions with natural scales.

For this set, we take α_s as given by equation (14) and $\Lambda = 190$ MeV, corresponding to the set of structure functions we will use [4, 5].

3.3.1 Definition

We assume for this case an SU(2) symmetry:

$$D_u^{\pi^0}(z, M_{f0}^2) = D_{\bar{u}}^{\pi^0}(z, M_{f0}^2) = D_d^{\pi^0}(z, M_{f0}^2) = D_{\bar{d}}^{\pi^0}(z, M_{f0}^2) = D_V(z, M_{f0}^2) + D_S(z, M_{f0}^2). \quad (22)$$

Then, we take

$$D_s^{\pi^0}(z, M_{f0}^2) = D_{\bar{s}}^{\pi^0}(z, M_{f0}^2) = D_c^{\pi^0}(z, M_{f0}^2) = D_{\bar{c}}^{\pi^0}(z, M_{f0}^2) = D_S(z, M_{f0}^2), \quad (23)$$

and

$$D_g^{\pi^0}(z, M_{f0}^2) = D_G(z, M_{f0}^2). \quad (24)$$

We parametrize the different functions of z as follows

$$D_V(z, M_{f0}^2) = N_v (1 - z)^{\beta_v} \quad (25)$$

$$D_S(z, M_{f0}^2) = N_s (1 - z)^{\beta_s} \quad (26)$$

$$D_G(z, M_{f0}^2) = N_g (1 - z)^{\beta_g}. \quad (27)$$

At the initial scale M_{f0} , we start with four flavors. The b quark contribution is taken into account in the evolution. Fixing the threshold at $4 m_b^2$, so we have:

$$D_b^{\pi^0}(z, M_f^2) = \begin{cases} 0 & \text{if } M_f^2 < 4m_b^2 \\ N_s (1 - z)^{\beta_s} & \text{if } M_f^2 = 4m_b^2 \end{cases} \quad (28)$$

So we are left with six parameters to be determined with the help of experimental data.

3.3.2 Choice of the scale

We use the standard approach to fix all the scales to the same value which is some natural scale of the problem. More precisely, for e^+e^- collisions, we take $\mu = M_f = \sqrt{S}$ whereas for $p p$ collisions, we set the three scales equal and proportional to the transverse momentum of the π^0 :

$$\mu = M = M_f = cP_t$$

where c is a constant to be fixed by the fit to experimental data .

3.3.3 Results for set I

First of all, for e^+e^- collisions, we limit ourselves to a π^0 energy greater than 2 GeV because we don't trust perturbation theory for low π^0 energies. Therefore for $\sqrt{S} \simeq 30$ GeV, we will only use z values greater than 0.1. As it can be inferred from eqs (25-27) we have not used a factor z^α in the input parametrizations since in this z range it does not improve the fit but only leads to correlations. With six parameters, a big correlation still occurs between N_v and β_v , so we fix $\beta_v = 1$. Then N_s , N_g and β_g remain slightly correlated. A good fit to CELLO [15], TASSO [16], TPC [17] and JADE [18] data leading to a $\chi^2 = 26.3$ for 29 points is obtained for values of the parameters given in table IV (systematic errors have been added in quadrature to statistical errors).

Using set I of fragmentation functions we will now evaluate the NLO cross-sections for inclusive π^0 production in hadronic collisions and compare them to experimental data from low center of mass energies up to the CERN collider one. Here, the situation is less clear. First, if we keep constant the value of the parameter c it is impossible to obtain a good fit in the whole energy domain. For example, setting $c \simeq 1.5$, the ISR data can be described but the

theoretical predictions are by far too low for WA70 and E706 and too high for UA2. A simple solution to this problem is to allow c to vary with the hadronic kinematical variables, in particular \sqrt{S} . A correct description of the data requires $c \simeq 0.39$ for WA70 [19] (see figure 8a), $c \simeq 0.5$ for E706 [20] (see figure 8b), $c \simeq 1.5$ for ISR experiment [21, 22] (see figure 8c) and $c \simeq 5.5$ for UA2 [23] (see figure 8d). In particular for the ISR energy range, the data from AFS collaboration [21] are marginally consistent with those of reference [22] since the transverse momentum dependence in the two experiments is different. Therefore it is very difficult to describe both ISR data with high precision. We get rather good fits of data of Kourkouvelis et al. [22] with $\chi^2 = 20.6$ for 14 points using $\mu = M = M_f = 1.3P_t$ and of the AFS collaboration [21] with $\chi^2 = 12.2$ for 11 points using $\mu = M = M_f = 1.6P_t$. Notice that the slope of the UA2 data is not correctly reproduced, with a $\chi^2 = 50.2$ for 11 points. The χ^2 have been calculated with statistical errors, allowing the overall normalization to vary within the systematic error.

A comment is in order here. The approach followed so far is rather simple. When the energy grows up the scales needed to describe data have also to increase. As stated above an acceptable fit of UA2 data [23] in the forward direction can be obtained for the choice of scales $\mu = M = M_f = 5.5P_t$ which is a priori a large scale. The compensation occurring between the leading and next-to-leading terms concerning the scale dependence is much more effective at high energies. At low energy, since we prevent the scale to be less than $M_{f0} = \sqrt{2}$ GeV, this compensation does not occur and the behavior of the leading and next-to-leading cross-sections is quite the same. In other words, we are not in a good region to perform perturbation theory.

This approach might be criticized. Indeed it is not very predictive, since the scales change with the energy. In other words one adds a new parameter which acts as an overall normalization for each experiment. Notice that the normalization of the glue fragmentation function N_g is strongly correlated to the choice made for the scale. More precisely, we could perfectly find a value for N_g which describes the UA2 data with $c = 0.5$. But in this case we couldn't describe the other data at lower energies.

3.4 Set II: fragmentation functions with optimized scales.

For this set, we take the numerical solution of equation (15) for α_s and $\Lambda = 230$ MeV, since we will use the ABFOW set of structure functions [6].

3.4.1 Definition

We assume also for this case an SU(2) symmetry:

$$D_u^{\pi^0}(z, M_{f0}^2) = D_{\bar{u}}^{\pi^0}(z, M_{f0}^2) = D_d^{\pi^0}(z, M_{f0}^2) = D_{\bar{d}}^{\pi^0}(z, M_{f0}^2) = D_u(z, M_{f0}^2). \quad (29)$$

Then we take:

$$D_s^{\pi^0}(z, M_{f0}^2) = D_{\bar{s}}^{\pi^0}(z, M_{f0}^2) = D_s(z, M_{f0}^2), \quad (30)$$

$$D_c^{\pi^0}(z, M_{f0}^2) = D_c^{\pi^0}(z, M_{f0}^2) = D_c(z, M_{f0}^2), \quad (31)$$

and

$$D_g^{\pi^0}(z, M_{f0}^2) = D_g(z, M_{f0}^2). \quad (32)$$

We parametrize these different functions of z in the following way:

$$D_u(z, M_{f0}^2) = N_u z^{-1} (1-z)^{\beta_u} \quad (33)$$

$$D_s(z, M_{f0}^2) = N_s z^{-1} (1-z)^{\beta_s} \quad (34)$$

$$D_c(z, M_{f0}^2) = N_c z^{-1} (1-z)^{\beta_c} \quad (35)$$

$$D_g(z, M_{f0}^2) = N_g z^{-1} (1-z)^{\beta_g}. \quad (36)$$

So we are left with eight parameters to be determined with the help of experimental data. Since we will use the optimized procedure for the determination of the scales, it is much simpler not to change the number of flavors. So, in this case, we will neglect the b contribution. This assumption is motivated by the fact that $\sigma(e^+ e^- \rightarrow \gamma^* \rightarrow b \bar{b}) = 1/4 \sigma(e^+ e^- \rightarrow \gamma^* \rightarrow c \bar{c})$ and in pp collision the b production is suppressed due to the weak b content of the proton.

A few remarks are in order here. As in the case of set I, the non singlet part D_i^- is always zero due to our assumptions. We did not take $D_s^{\pi^0} = D_c^{\pi^0}$ because in this case the sum over the four flavors of D_i^+ weighted by the square electric charge is zero:

$$\sum_{i=u,d,s,c} e_i^2 \left(D_i^+(z, M^2) + D_{\bar{i}}^+(z, M^2) \right) = 0.$$

So, there is no non-singlet contribution to the cross-section. Therefore we could parametrize directly the singlet and the glue with four parameters only. The e^+e^- data could be correctly described, but the glue is very constrained and it will not be possible to fit hadronic data in the whole energy range.

3.4.2 Choice of the scale

For set II, we use optimized scales according to the procedure of Politzer and Stevenson [28]. Concerning e^+e^- collisions, our approach is the following. Firstly since the scale μ does not appear at lowest order, we cannot optimize with respect to it. Therefore we set $\mu = M_f$ and perform an optimization only with respect to the scale M_f . Therefore, a priori, our optimized scale depends on the choice made for the input fragmentation functions. We have not found a way to get rid from this sensitivity. In practice, the optimized point changes slowly when the input is modified and in addition, since we are in a stable region, it does not matter if we are not exactly on the optimized point. The optimized scale M_f^{opt} is of order of $\sqrt{S}/8$ varying slowly with z . Furthermore, we find no optimization scale for $z \leq .03$ for $\sqrt{S} = 35$ GeV, $z \leq .05$ for $\sqrt{S} = 29$ GeV and $z \leq .1$ for $\sqrt{S} = 22$ GeV. For lower values of \sqrt{S} , it is not possible to optimize.

We also use an optimization procedure for hadronic collisions. So we require that:

$$\frac{\partial}{\partial \ln(\mu^2/\Lambda^2)} E_{\pi^0} \frac{d\sigma_{p+p \rightarrow \pi^0}}{d^3 \vec{P}_{\pi^0}} = 0 \quad (37)$$

$$\frac{\partial}{\partial \ln(M^2/\Lambda^2)} E_{\pi^0} \frac{d\sigma_{p+p \rightarrow \pi^0}}{d^3 \vec{P}_{\pi^0}} = 0 \quad (38)$$

$$\frac{\partial}{\partial \ln(M_f^2/\Lambda^2)} E_{\pi^0} \frac{d\sigma_{p+p \rightarrow \pi^0}}{d^3 \vec{P}_{\pi^0}} = 0. \quad (39)$$

The first equation can be computed analytically:

$$\begin{aligned} \frac{\partial}{\partial \ln(\mu^2/\Lambda^2)} E_{\pi^0} \frac{d\sigma_{p+p \rightarrow \pi^0}}{d^3 \vec{P}_{\pi^0}} = & -\alpha_s^4(\mu^2) b \left\{ 2b' A + 3(1 + b' \alpha_s(\mu^2)) \left[2bA \ln\left(\frac{\mu^2}{\Lambda^2}\right) \right. \right. \\ & \left. \left. + B \ln\left(\frac{M^2}{\Lambda^2}\right) + C \ln\left(\frac{M_f^2}{\Lambda^2}\right) + D \right] \right\} \quad (40) \end{aligned}$$

having used

$$\frac{\partial \alpha_s(\mu^2)}{\partial \ln(\mu^2/\Lambda^2)} = -b \alpha_s^2(\mu^2) (1 + b' \alpha_s(\mu^2)). \quad (41)$$

Note that terms of order of α_s^3 have been cancelled as it should be. Now, we determine the scale μ in order to cancel the right-hand side of eq (40). This ensures us that the corrective term K will be negative with a magnitude of roughly 10 % of the lowest order. Then we compute numerically the value of the scales M and M_f which have to fulfill the equations (38) (39), the scale μ being now a function of M , M_f . We require that the factorization scales must be greater than $\sqrt{2}$ GeV and that the renormalization scale is such that the running coupling constant α_s is less than .34. With these constraints it will be impossible to optimize in low P_t range. More precisely, for low center of mass energies ($\sqrt{S} \leq 63$ GeV), the optimization is not possible for $P_t \leq 5$ GeV. Therefore these regions are not appropriate to apply an optimization procedure.

3.4.3 Results for set II

First we freeze β_s , β_c and β_g according to the counting rules. There are still too many parameters, so we fix N_g and fit to e^+e^- data with four parameters N_u , β_u , N_s and N_c . The fragmentation functions extracted are then used to evaluate hadronic cross sections. Then we vary N_g refitting e^+e^- data and apply the new input to pp data. This procedure is repeated until a reasonable description of hadronic data is reached. Good fits of e^+e^- data (CELLO [14, 15], TASSO [16], TPC [17] and JADE [18]) leading to a $\chi^2 \simeq 1$ per d.o.f. are obtained for the two sets - hereafter denoted as set IIa and set IIb - displayed in Table V and Table VI (see figures 9 and 10 using set IIb). The two sets differ mainly for the gluon normalization. As can be seen from inspection of figures 11a, 11b, 12a and 12b a rather good fit of the latest UA2 data at $\sqrt{S} = 630$ GeV [23], AFS [21] and Kourkouvelis et al data [22] can be obtained leading to a $\chi^2 \simeq 50$ for 31 points. Kourkouvelis et al. data favor the set characterized

by the largest glue (set IIb) whereas UA2 data are better fitted by the other set (set IIa). Notice that we have taken into account the systematic errors of the data which affect the overall normalization. The χ^2 are 3.46 (4.28) for the 11 AFS points, 31.54 (23.52) for the 9 Kourkouvelis et al. points and 14.91 (20.00) for the 11 UA2 points with the parameters of set IIa (IIb). Inside the systematic errors we can also describe UA2 data at $\sqrt{S} = 540$ GeV and $\eta = 1.4$. On the other hand we are not able to describe WA70 and E706 data with the values of N_g found before. This is not very surprising since the corrective term is found to be huge, and although we can find an optimization point this is not very stable suggesting that we are not in the appropriate region to trust perturbation theory.

4 Predictions at future hadron colliders.

As we have seen present data do not allow to extract the π^0 fragmentation functions unequivocally. To this aim the forthcoming information from *ep* HERA collider should be very helpful. With these limitations we will now estimate the π^0 rates at LHC using the various sets of fragmentation functions previously derived.

Let us consider first set I of fragmentation functions. In order to describe hadronic data we had to increase the scales $\mu = M = M_f$ from $\frac{P_t}{2}$ at $\sqrt{S} \simeq 20$ GeV up to $5P_t$ at $\sqrt{S} = 630$ GeV. An extrapolation to LHC energy would lead to $\mu = M = M_f \simeq 50P_t$ which seems by far an unnatural scale. To estimate the sensitivity to scales we show in figure 13 the ratio of cross sections at LHC for the two scales $50P_t$ and P_t at $\eta = 0$. As can be inferred from the figure the rates differ by at most a factor of two. To estimate the uncertainty due to structure functions we have taken the set of structure functions of HMRS [5] using the \overline{MS} scheme and the set of Morfing-Tung [4] using the DIS scheme. The predictions differ by at most 20%. Similarly the ratio of predictions using set II is displayed in figure 14.

Finally the ratio of the two predictions from the HERWIG fragmentation functions, for $\delta = 0.35, 0.40$, evolved to NLO accuracy as discussed in section 3.2, are displayed in figure 15.

The situation is summarized in figure 16 where we show the absolute rates at LHC for $\eta = 0$ from the most plausible sets in the three approaches. This gives an estimate of the theoretical uncertainty which is of the order of a factor two. The uncertainty on structure functions is marginal compared to the poor determination of fragmentation functions.

To show the stability of the NLO corrections we display the cross section as a function of the scales μ and $M = M_f$ compared to the LO result for $P_t = 50$ GeV (figures 17) and for $P_t = 200$ GeV (figures 18). We vary the scales between $P_t/5$ and $5P_t$. The NLO cross sections exhibit a saddle point whereas the LO cross sections decrease monotonically when the scales increase.

The uncertainty due to factorisation scheme, especially coming from fragmentation functions is expected to be tiny for the two following reasons. Firstly the evaluation done for one jet inclusive cross section has shown[2] that at collider energies its magnitude is of the order of 5% -if done correctly - and we can reasonably expect a same order of magnitude for one hadron inclusive cross section. Secondly a precise estimate doesn't seem mandatory compared to the large uncertainty coming from fragmentation functions.

5 Conclusions

We have performed a complete next to leading order analysis of inclusive π^0 production from e^+e^- and hadronic data. For the first time an attempt to extract sets of π^0 fragmentation functions at NLO has been performed. The present quality of data does not allow us to derive a unique set fitting all experimental data. For this purpose more accurate measurements from hadronic colliders in the large P_t domain, from e^+e^- colliders in the large z_H domain as well as complementary information from ep collisions will be very helpful. The theoretical uncertainties are mainly due to the poorly determined fragmentation functions. Nevertheless the absolute rates at future colliders like LHC and SSC can be predicted within a factor of two. This will certainly be of help for neutral background rejection at supercolliders.

Note added in proof

After completion of this work the paper "Higher order QCD corrections to inclusive particle production in $p\bar{p}$ collision" by F. M. Borzumati et al. [29] has appeared, where the π^0 inclusive production has been discussed, using the old LO fragmentation functions of ref.[8] and the NLO results of our group [2].

Acknowledgements

We would like to thank P. Nason for providing us his fortran code for b fragmentation at next to leading order. We are greatly indebted to G. Marchesini for enlightening discussions concerning HERWIG and also to P. Aurenche for advice on optimization procedure. We acknowledge discussions on the ISR data with C. Kourkouvelis.

Table captions

- Table I: average fraction of energy of the fragmenting parton (see eq.18) from pp collisions.
- Table II: parameters of the quark fragmentation functions (see eq.20) as obtained from HERWIG in e^+e^- annihilation at $M_0 = 30$ GeV.
- Table III: parameters of the gluon fragmentation functions (see eq.20) as obtained from HERWIG at $M_0 = 30$ GeV, with two hypotheses on the angle δ (see text).
- Table IV: parameters for the π^0 fragmentation functions (set I) obtained from e^+e^- annihilation.
- Table V: parameters for the π^0 fragmentation functions (set IIa) obtained from optimization procedure in e^+e^- annihilation.
- Table VI. Parameters for the π^0 fragmentation functions (set IIb) obtained from optimization procedure in e^+e^- annihilation.

$\sqrt{S} = 23 \text{ GeV}$ and $\eta = 0.$		$\sqrt{S} = 63 \text{ GeV}$ and $\eta = 0.$		$\sqrt{S} = 630 \text{ GeV}$ and $\eta = 1.4$	
$P_t^{\pi^0}$	$\langle z \rangle$	$P_t^{\pi^0}$	$\langle z \rangle$	$P_t^{\pi^0}$	$\langle z \rangle$
4.11	0.81	5.25	0.67	13	0.55
4.61	0.82	6.73	0.70	21	0.60
5.69	0.86	8.23	0.73	29.8	0.65
6.69	0.89	10.4	0.77	43.7	0.74

Table I

<i>Process</i>	α	β	N_q	$\langle n_\pi \rangle$
$e^+e^- \rightarrow u\bar{u}$	-0.95 ± 0.02	3.67 ± 0.19	1.20	2.95
$e^+e^- \rightarrow d\bar{d}$	-0.95 ± 0.02	3.67 ± 0.15	1.24	2.87
$e^+e^- \rightarrow s\bar{s}$	-0.88 ± 0.02	5.32 ± 0.23	1.68	2.73
$e^+e^- \rightarrow c\bar{c}$	-0.82 ± 0.02	8.02 ± 0.24	3.09	3.42
$e^+e^- \rightarrow b\bar{b}$	-0.95 ± 0.02	10.94 ± 0.29	2.92	4.20

Table II

δ	α	β	N_g	$\langle n_\pi \rangle$
0.35 rad	-0.28 ± 0.04	6.71 ± 0.39	14.49	3.65
0.4 rad	-0.37 ± 0.04	5.79 ± 0.36	12.93	4.55

Table III

<i>Parton</i>	α_i	β_i	N_i
<i>valence</i>	0.	1.	0.19
<i>sea</i>	0.	5.2	3.5
<i>gluon</i>	0.	2.03	4.9

Table IV

<i>Parton</i>	α_i	β_i	N_i
<i>up</i>	-1.	0.94	0.11
<i>strange</i>	-1.	3.0	0.55
<i>charm</i>	-1.	4.	2.7
<i>gluon</i>	-1.	2.	0.55

Table V

<i>Parton</i>	α_i	β_i	N_i
<i>up</i>	-1.	1.11	0.15
<i>strange</i>	-1.	3.0	0.18
<i>charm</i>	-1.	4.	2.5
<i>gluon</i>	-1.	2.	0.75

Table VI

Figure Captions

- Fig. 1: relative inclusive partonic production in hadronic collisions as a function of the partonic transverse momentum $P_{t\ell}$ at various energies: WA70 experiment(fig 1a), ISR experiments(fig 1b),UA2(fig 1c) and LHC(fig 1d). The various curves refer to: $pp \rightarrow u+d$ (full line), $pp \rightarrow s+c$ (dashed line) and $pp \rightarrow g$ (dot-dashed line).
- Fig. 2: LO inclusive π^0 production in e^+e^- annihilation with the quark fragmentation functions extracted from HERWIG at $\sqrt{S} = 30$ GeV, compared with experimental data at $\sqrt{S} = 35$ GeV.
- Fig. 3: NLO inclusive π^0 production in e^+e^- annihilation with the quark and gluon fragmentation functions extracted from HERWIG and evolved at $\sqrt{S} = 35$ GeV, compared with data.
- Figs. 4: NLO inclusive π^0 production in pp collisions at ISR energies for $\mu = M = M_f = P_t, P_t/2$ for $\delta = 0.35$ (see text). The fragmentation functions are from HERWIG.
- Figs. 5: same as fig 4, for $\delta = 0.40$.
- Figs. 6: NLO inclusive π^0 production in $p\bar{p}$ collisions at $Spp\bar{S}$ energies for $\mu = M = M_f = P_t, P_t/2$ for $\delta = 0.35$ and $\delta = 0.40$, at $\sqrt{S} = 540$ GeV and $\eta = 0$. The fragmentation functions are from HERWIG.
- Figs. 7: same as fig 6 at $\sqrt{S} = 630$ GeV and $\eta = 1.4$.
- Figs. 8: NLO inclusive π^0 production in hadronic collisions with set I fragmentation functions (see text) for various energies. The scales $\mu = M = M_f = cP_t$ are indicated explicitly.
- Fig. 9: NLO inclusive π^0 production in e^+e^- annihilation with set II of fragmentation functions compared to CELLO, TASSO and JADE data. The gluon parameter N_g takes the value $N_g = 0.75$. Data and theory have been multiplied by 0.1 at $\sqrt{S} = 22$ GeV.
- Fig. 10: Same as fig 9 for TPC data.
- Figs. 11: NLO inclusive π^0 production in pp collisions with set II fragmentation functions (see text) at ISR energies (squares correspond to AFS data whereas circles correspond to Kourkoumelis et al data). The gluon parameter N_g takes the value $N_g = 0.55$ (fig 11a) and $N_g = 0.75$ (fig 11b).
- Figs. 12: same as fig 11 at $Spp\bar{S}$ energies.
- Fig. 13: ratio of inclusive π^0 cross sections predicted at LHC for $\eta = 0$ using set I of fragmentation functions with $\mu = M = M_f = 50P_t$ over $\mu = M = M_f = P_t$.

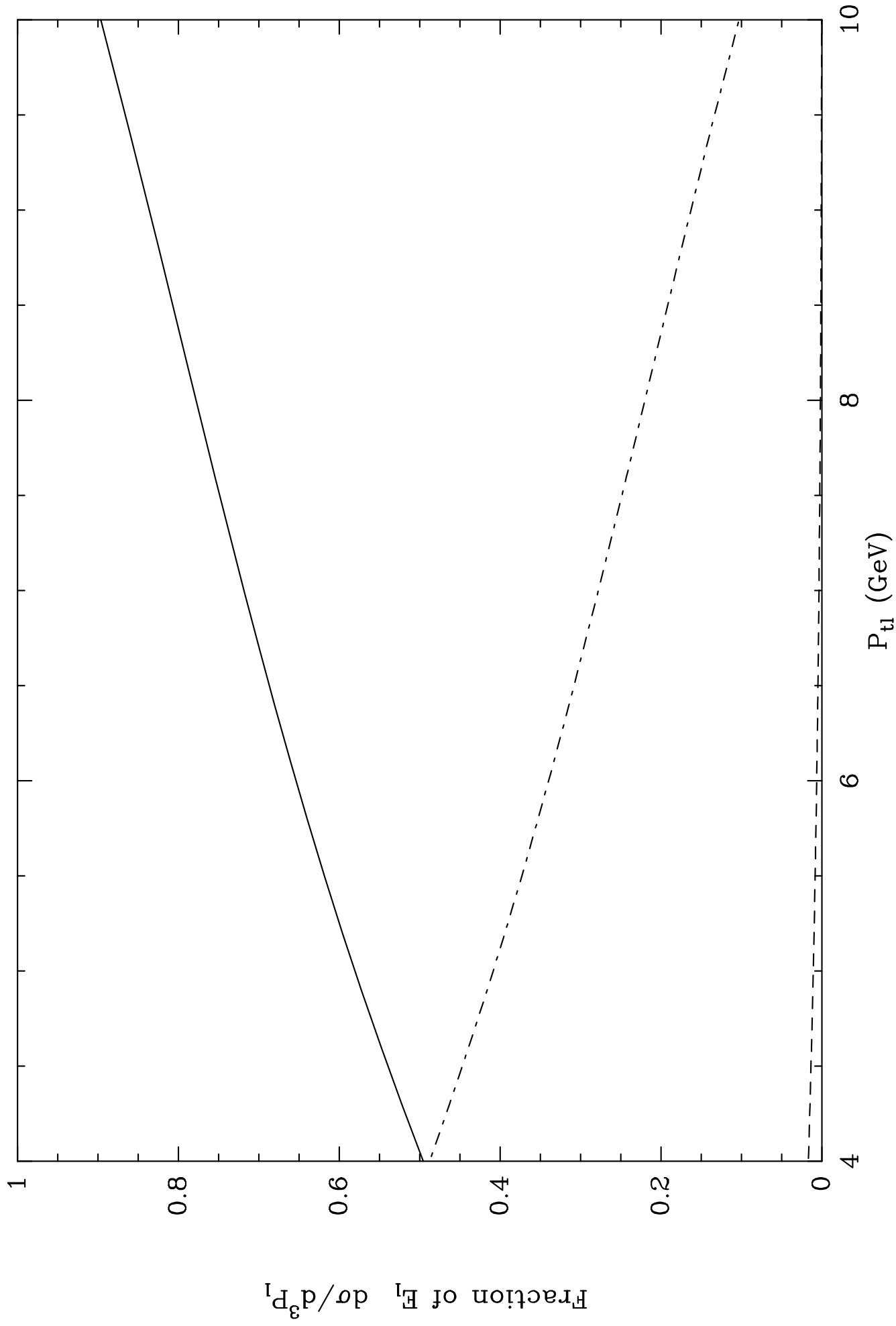
- Fig. 14: ratio of inclusive π^0 cross sections predicted at LHC for $\eta = 0$ using set IIb of fragmentation functions over set IIa .
- Figs. 15: ratio of inclusive π^0 cross sections predicted at LHC for $\eta = 0$ using fragmentation functions from HERWIG.
- Fig. 16: inclusive π^0 cross sections predicted at LHC for $\eta = 0$ using various fragmentation functions : HERWIG with $\delta = 0.35$ (full line), set I with $\mu = M = M_f = 50P_t$ (dot-dashed curve) and set II with $N_g = 0.75$ (dashed curve).
- Figs. 17: inclusive π^0 cross sections at LHC in pb using set I of fragmentation functions as a function of the scales μ and $M = M_f$ for $P_t = 50$ GeV and $\eta = 0$. LO prediction : fig 17a . NLO prediction : fig 17b.
- Figs. 18: same as fig 17 for $P_t = 200$ GeV and $\eta = 0$.

References

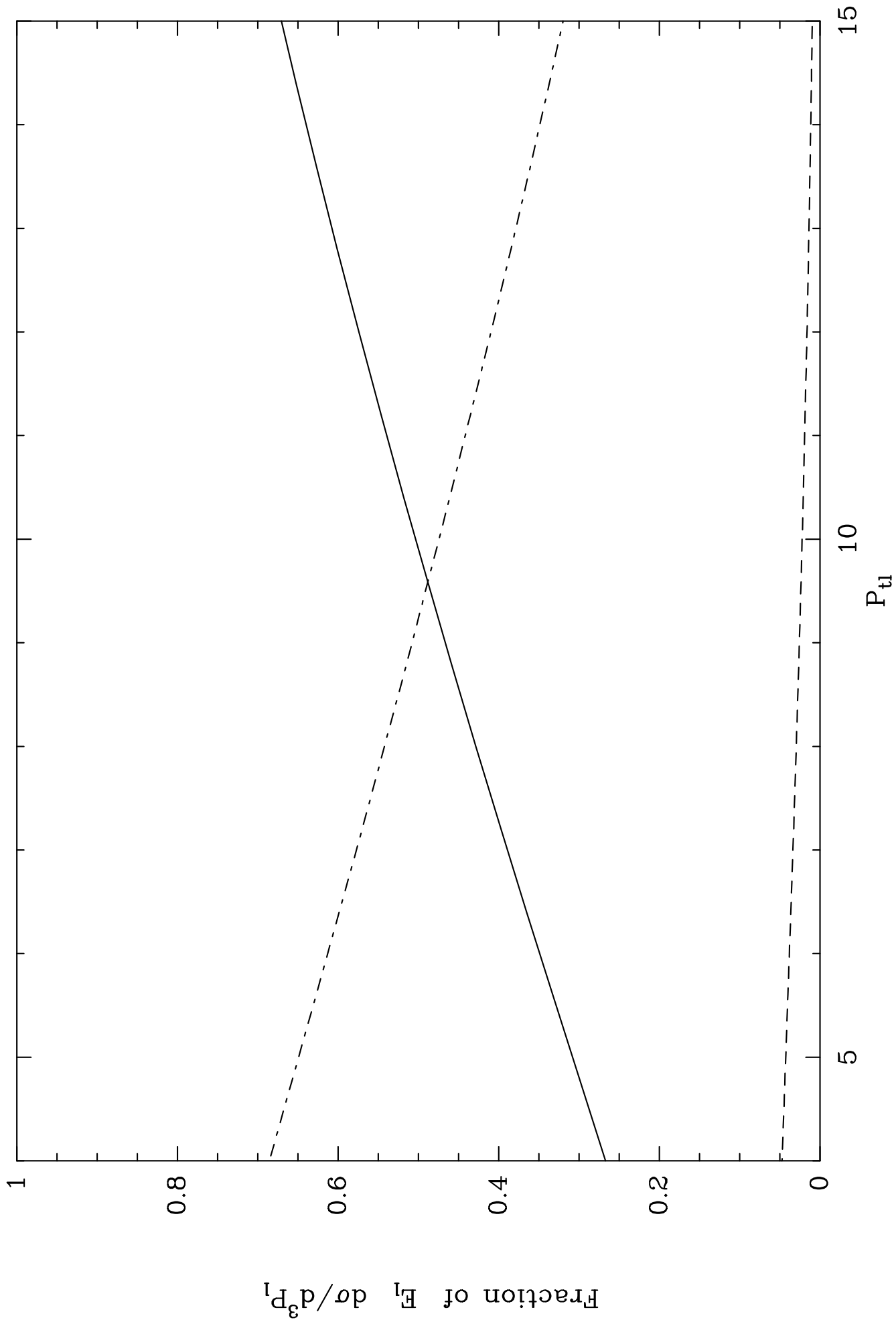
- [1] For a review see for example G. Altarelli, D. Denegri and F. Pauss, Proceedings of Aachen LHC Workshop vol 1 CERN 90-10, G. Jarlskog and D. Reineds.
- [2] F.Aversa, P.Chiappetta, M.Greco and J.Ph.Guillet, Nucl. Phys. B327, 105 (1989).
- [3] R.K. Ellis and J.C. Sexton, Nucl. Phys. B269, 445 (1986).
- [4] J. G. Morfin and W. K. Tung, Z. Phys. C52, 13 (1989).
- [5] A. D. Martin, R. G. Roberts and W. J. Stirling, Phys. Rev. D37, 1161 (1988); Mod. Phys. Lett A4, 1135 (1989); P. N. Harriman, A. D. Martin, R. G. Roberts and W. J. Stirling, Phys. Rev. D42, 798 (1990) and Phys. Rev. D42, 3645 (1990).
- [6] P. Aurenche, R. Baier, M. Fontannaz, J.F. Owens and M. Werlen, Phys. Rev. D39, 3275 (1989).
- [7] B. Mele and P. Nason, Nucl. Phys. B361, 626 (1991).
- [8] R. Baier, J. Engels and B. Petersson, Z. Phys. C2, 265 (1979); M. Anselmino, P. Kroll and E. Leader, Z. Phys. C18, 307 (1983).
- [9] G. Marchesini and B. R. Webber, Nucl. Phys. B238, 1 (1984); *ibidem* 310, 461 (1989) .
- [10] G. Altarelli and G. Parisi, Nucl. Phys. B126 (1977) 298.
- [11] G.Curci, W.Furmanski and R.Petronzio, Nucl. Phys. B175, 27 (1980).
- [12] G.Altarelli, R.K.Ellis, G.Martinelli and S.Y.Pi, Nucl. Phys B160, 301 (1979).
- [13] R.Baier and K.Fey, Z. Phys. C2 (1979) 339.
- [14] CELLO collab.: H. J. Behrend et al., Z. Phys. C20, 207 (1983).
- [15] CELLO collab.: H. J. Behrend et al., Z. Phys. C47, 1 (1990).
- [16] TASSO collab.: W. Braunschweig et al., Z. Phys. C33, 13 (1986).
- [17] TPC collab.: H. Aihara et al., Z. Phys. C27, 187 (1985).
- [18] JADE collab.: W. Bartel et al., Z. Phys. C28, 343 (1985).
- [19] WA70 collab.: M. Bonesini et al., Z. Phys. C38, 371 (1988).
- [20] E706 collab.: G. Alverson et al., Phys. Rev. D45, 3899 (1992).
- [21] AFS collab.: T. Akesson et al., Sov. J. Nucl. Phys. 51, 836 (1990).

- [22] C. Kourkouvelis et al., Z. Phys. C5, 95 (1980).
- [23] UA2 collab. 630 GeV: R. Ansari et al., Z. Phys. C41, 395 (1988); UA2 collab. 540 GeV: M. Banner et al., Z. Phys. C27, 329 (1985). ; M. Banner et al., Phys. Lett. B115, 59 (1982).
- [24] B.R. Webber, CERN-TH 6706/92 (1992).
- [25] ARGUS collab.: H. Albrecht et al., Z. Phys. C46, 15 (1990).
- [26] L3 Collaboration, Phys. Lett. B259, 199 (1991).
- [27] W.Furmanski and R.Petronzio, Phys. Lett. B97, 437 (1980).
- [28] P.M.Stevenson and H.D.Politzer, Nucl. Phys. B277, 758 (1986).
- [29] F.M.Borzumati, B.A.Kniehl, G.Kramer, preprint DESY 92-135, Oct.92

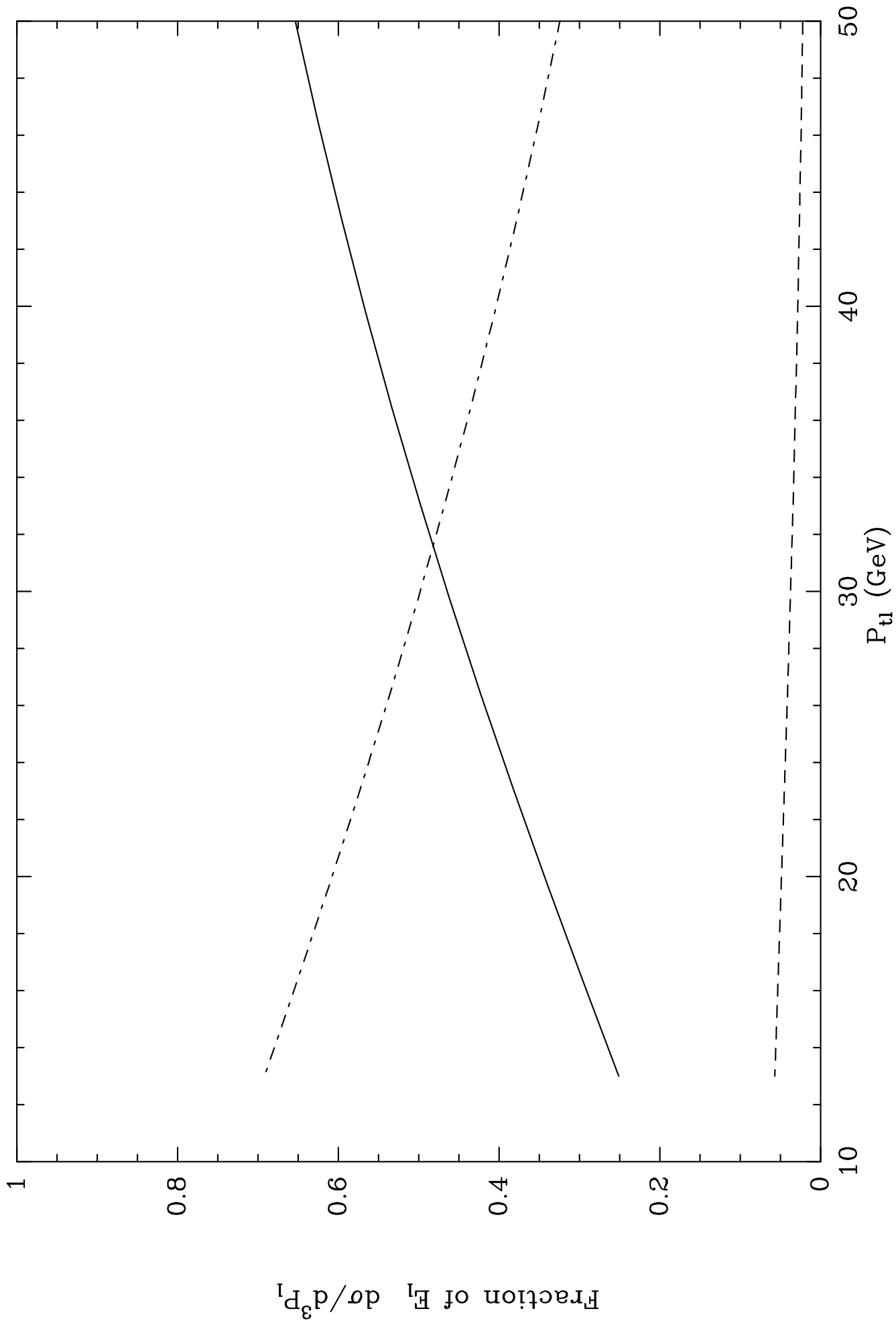
WA70:pp \rightarrow u+d(full),s+c+(b)(dashed),g(dot-dashed)



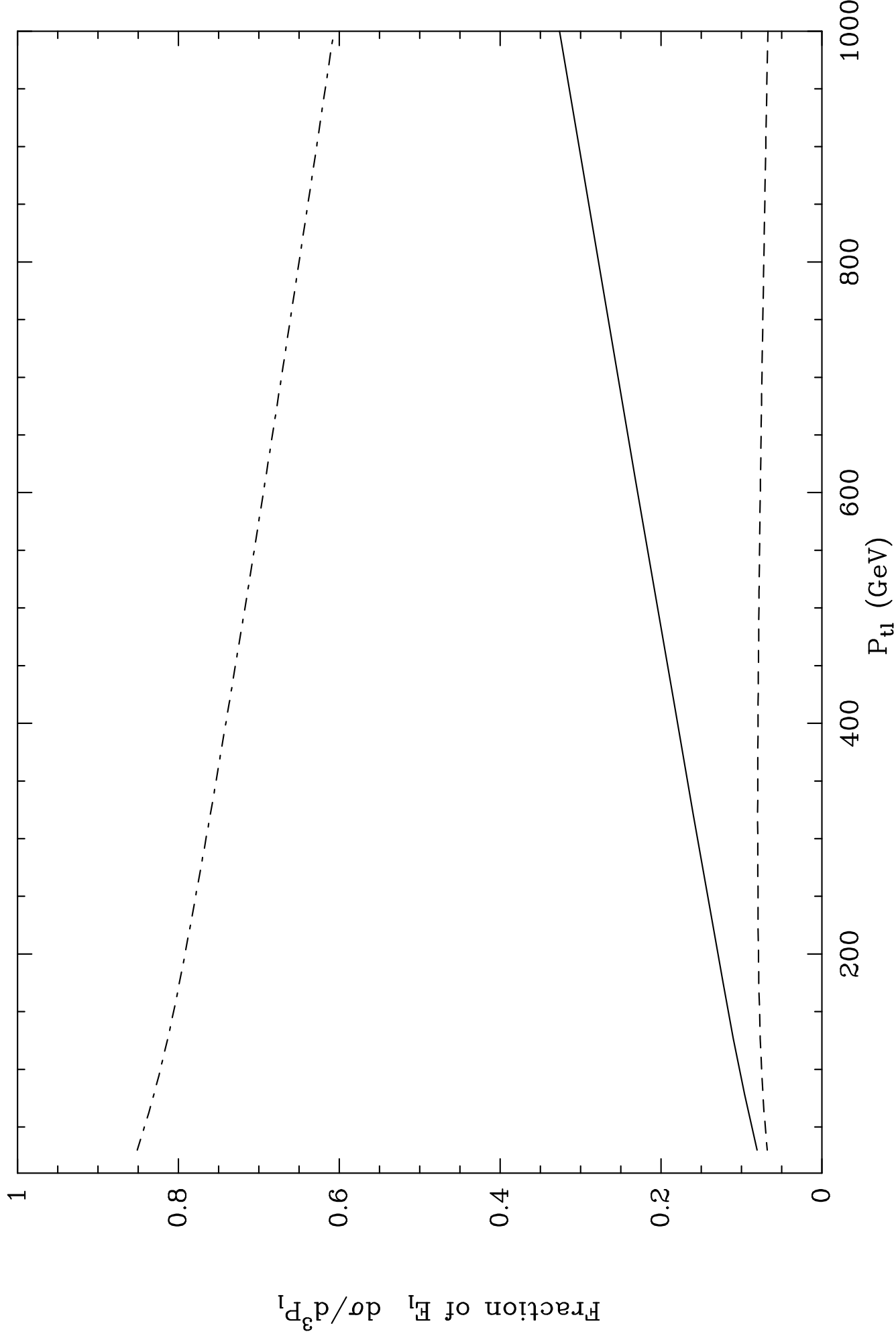
ISR:pp \rightarrow u+d(full),s+c+(b)(dashed),g(dot-dashed)

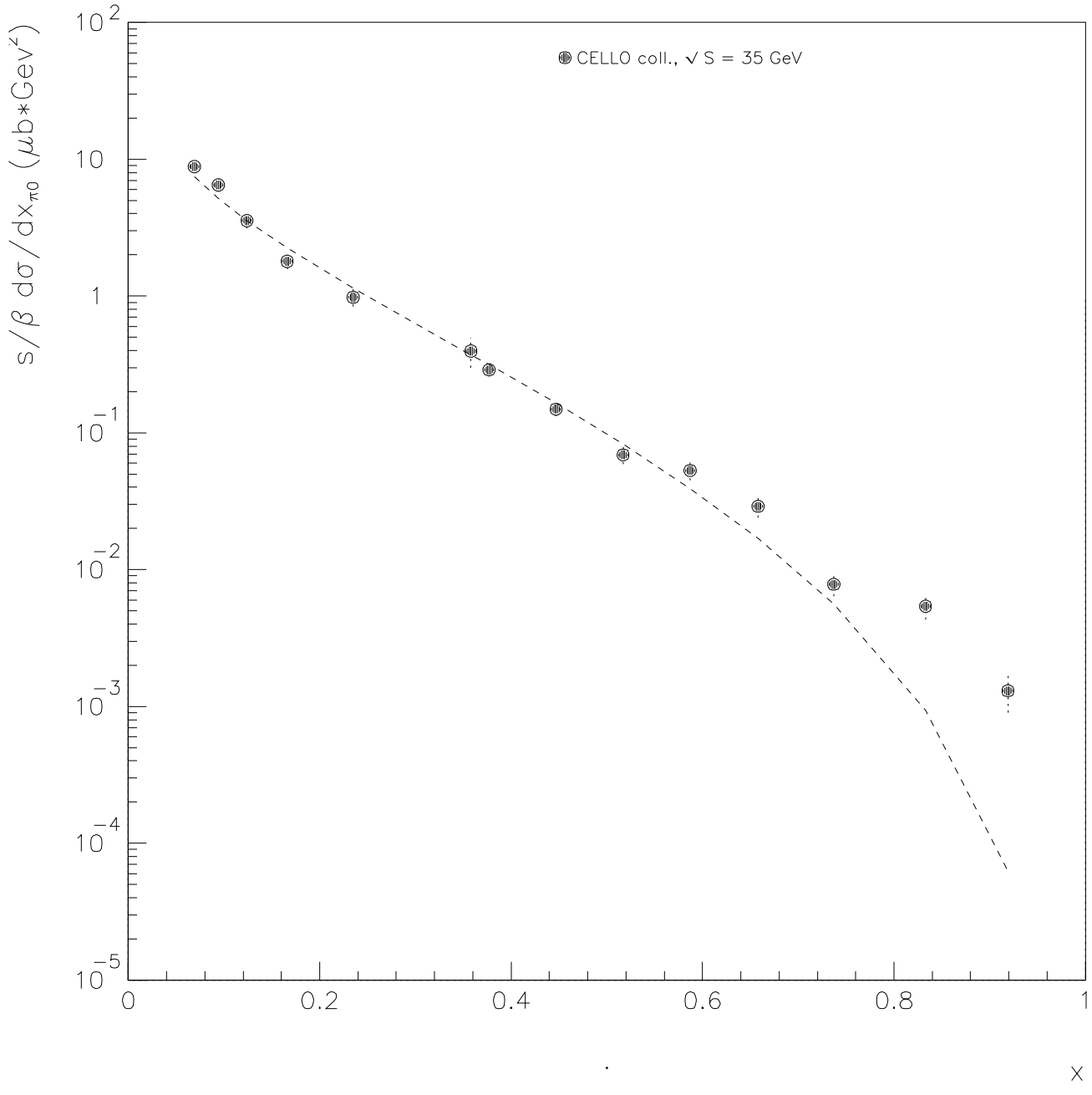


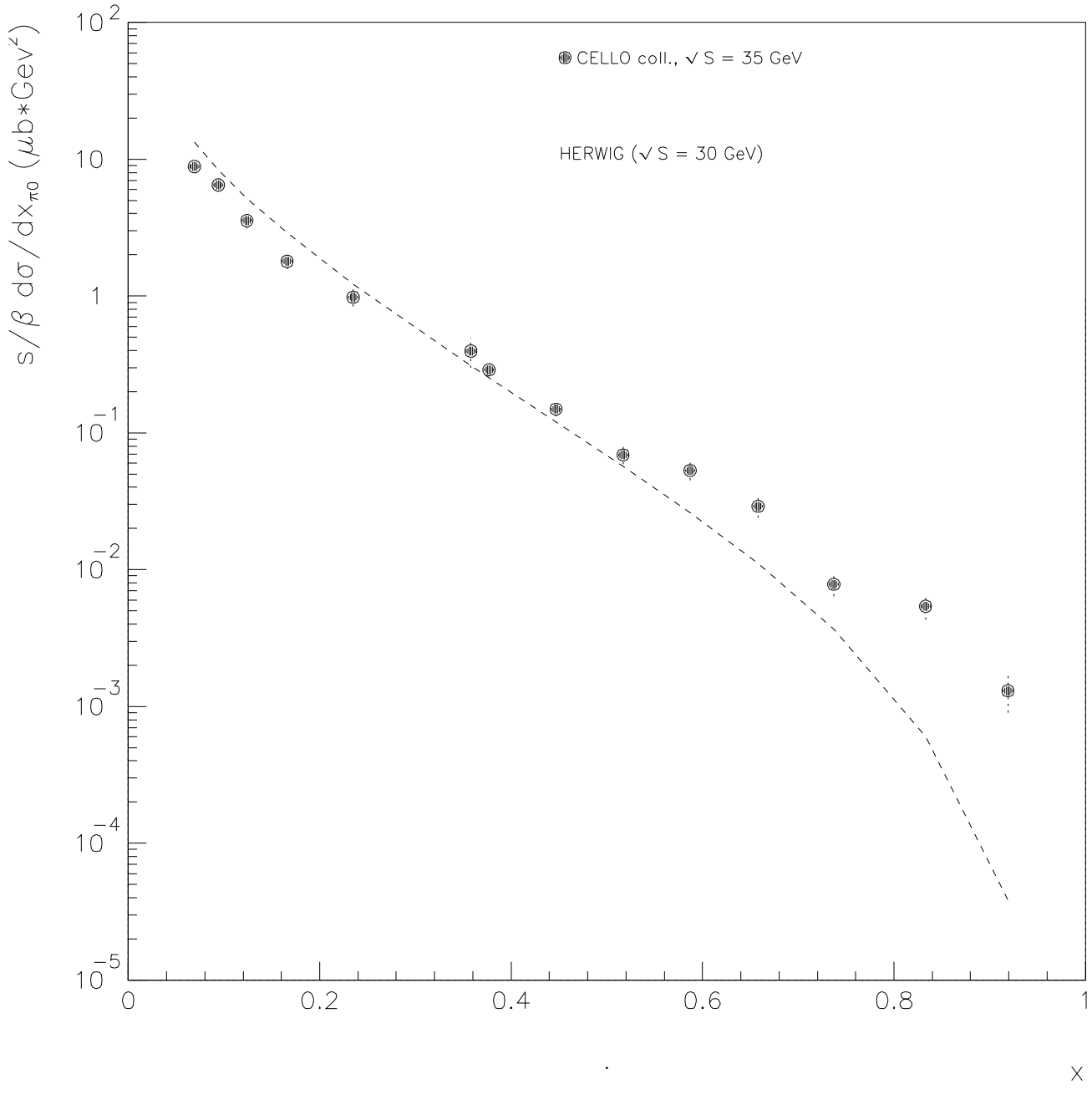
UA2:pp \rightarrow u+d (full),s+c (dashed),g (dot-dashed)

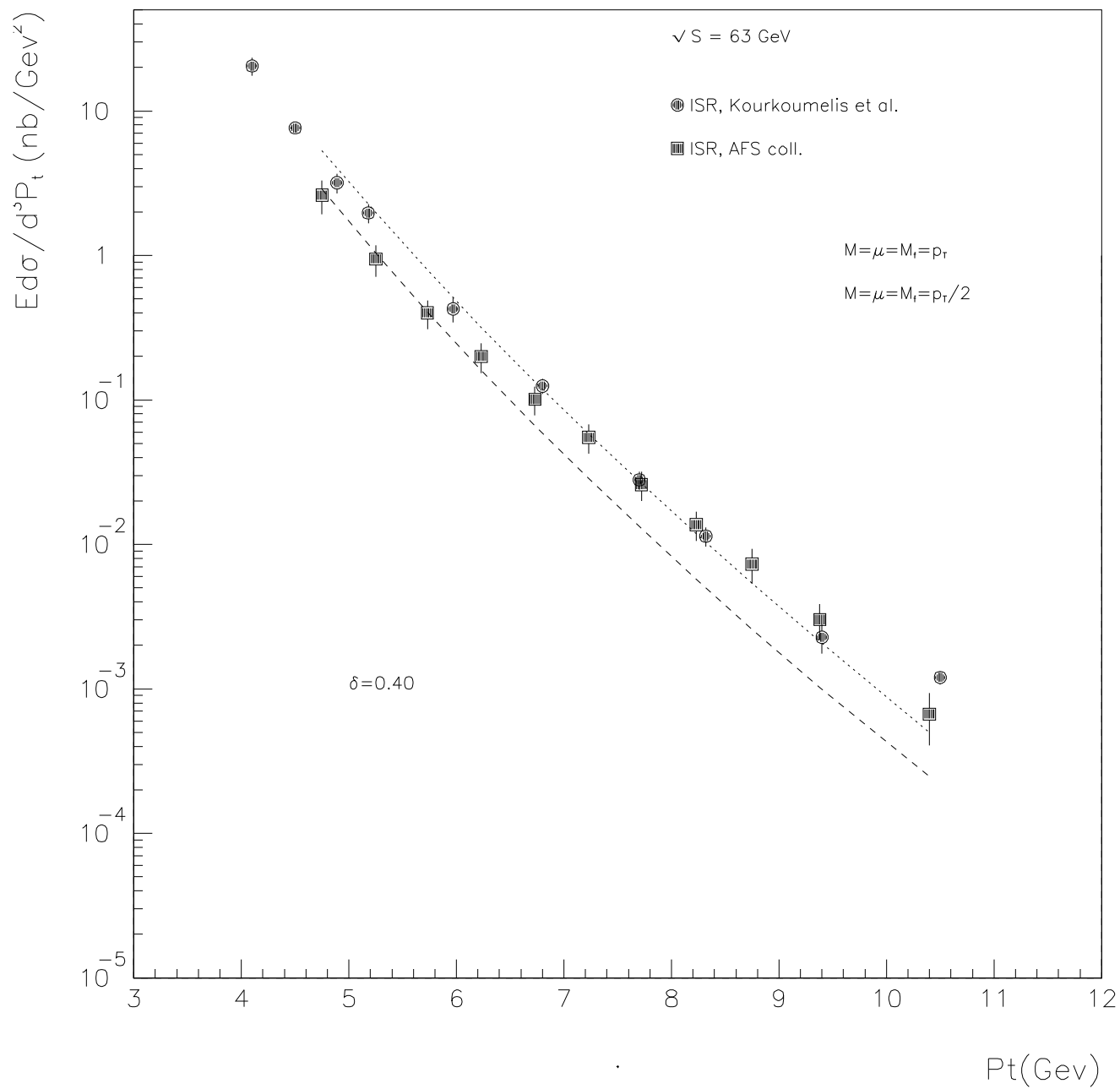


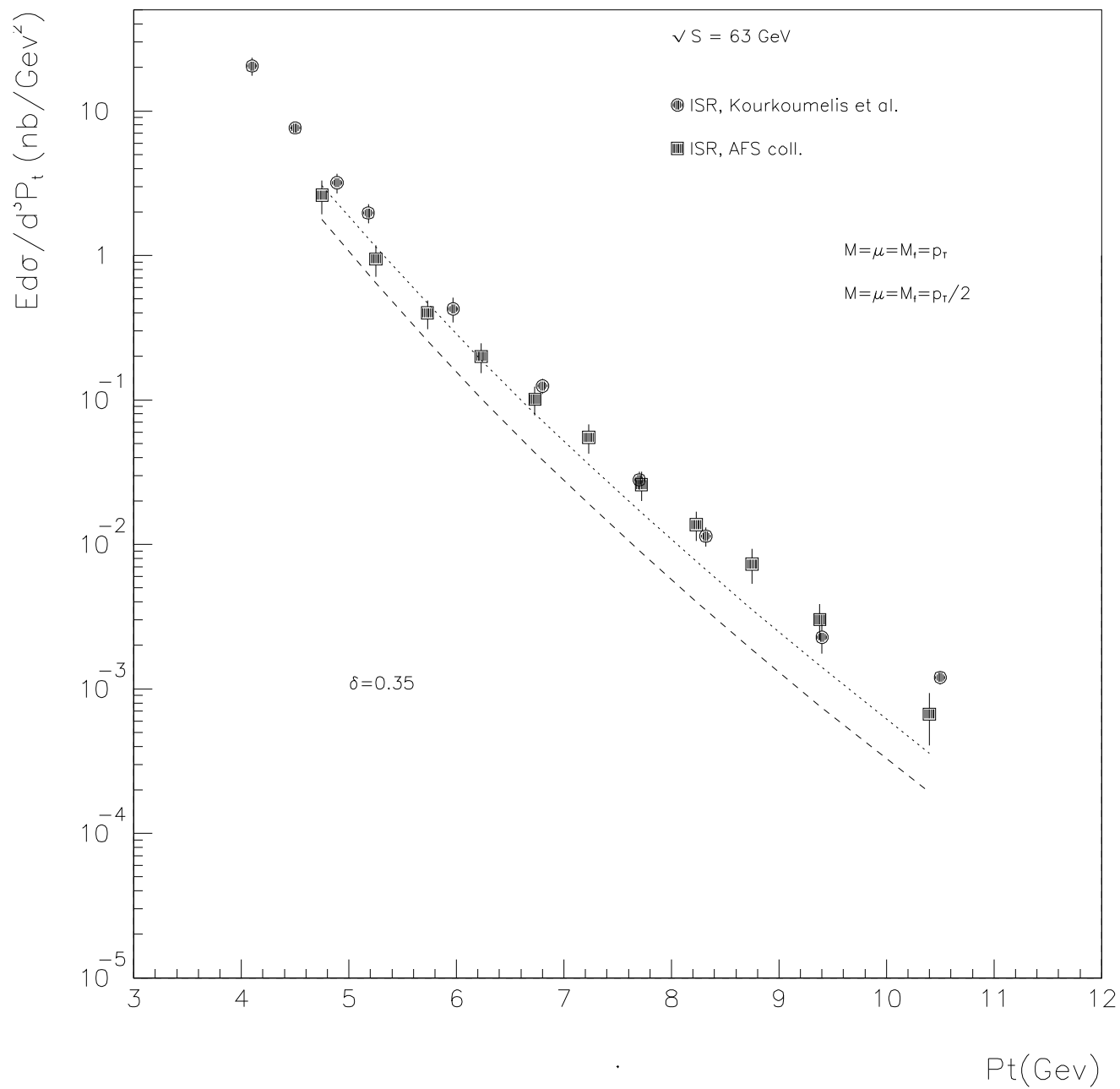
LHC:pp \rightarrow u+d (full),s+c (dashed),g (dot-dashed)

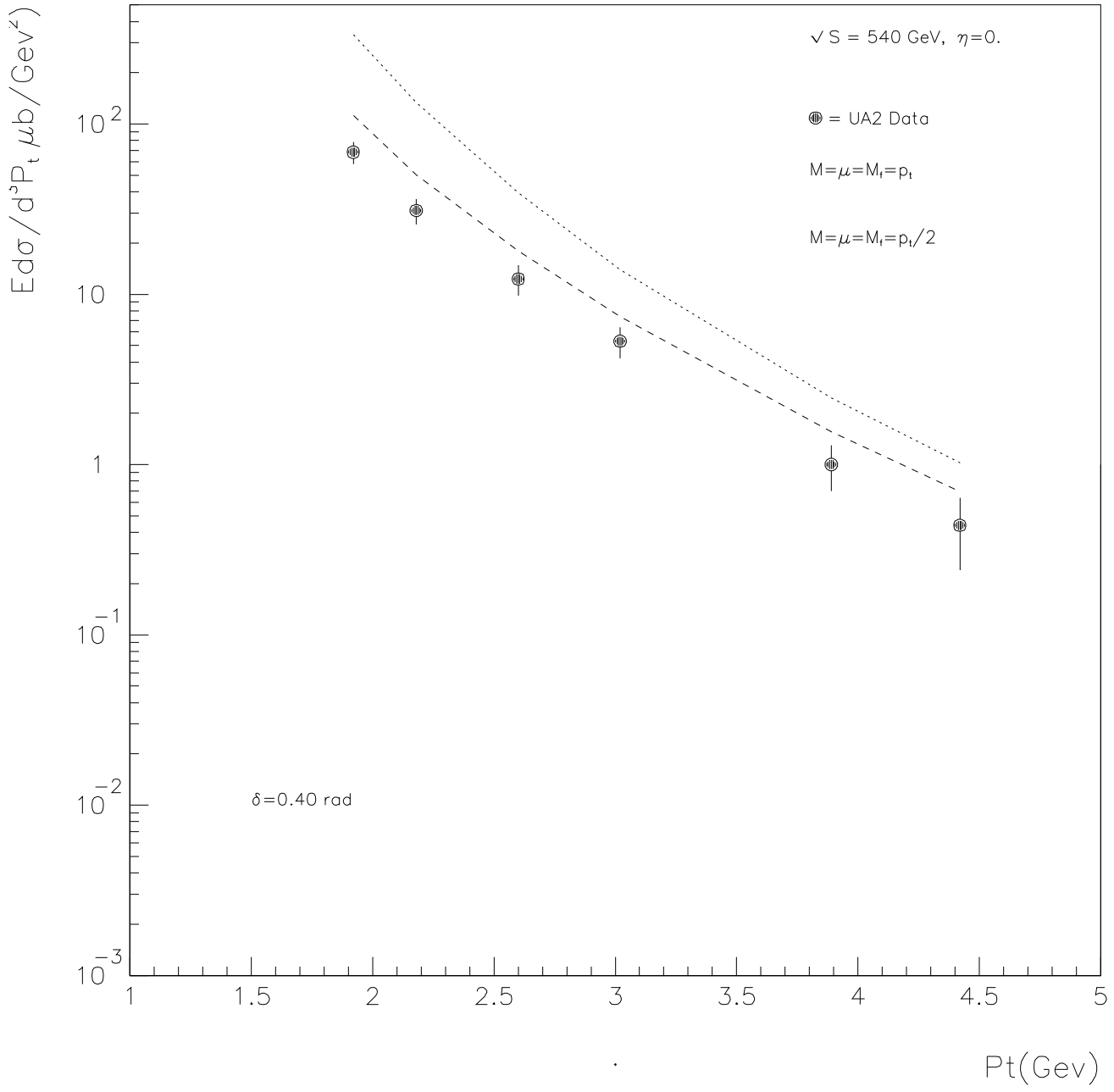


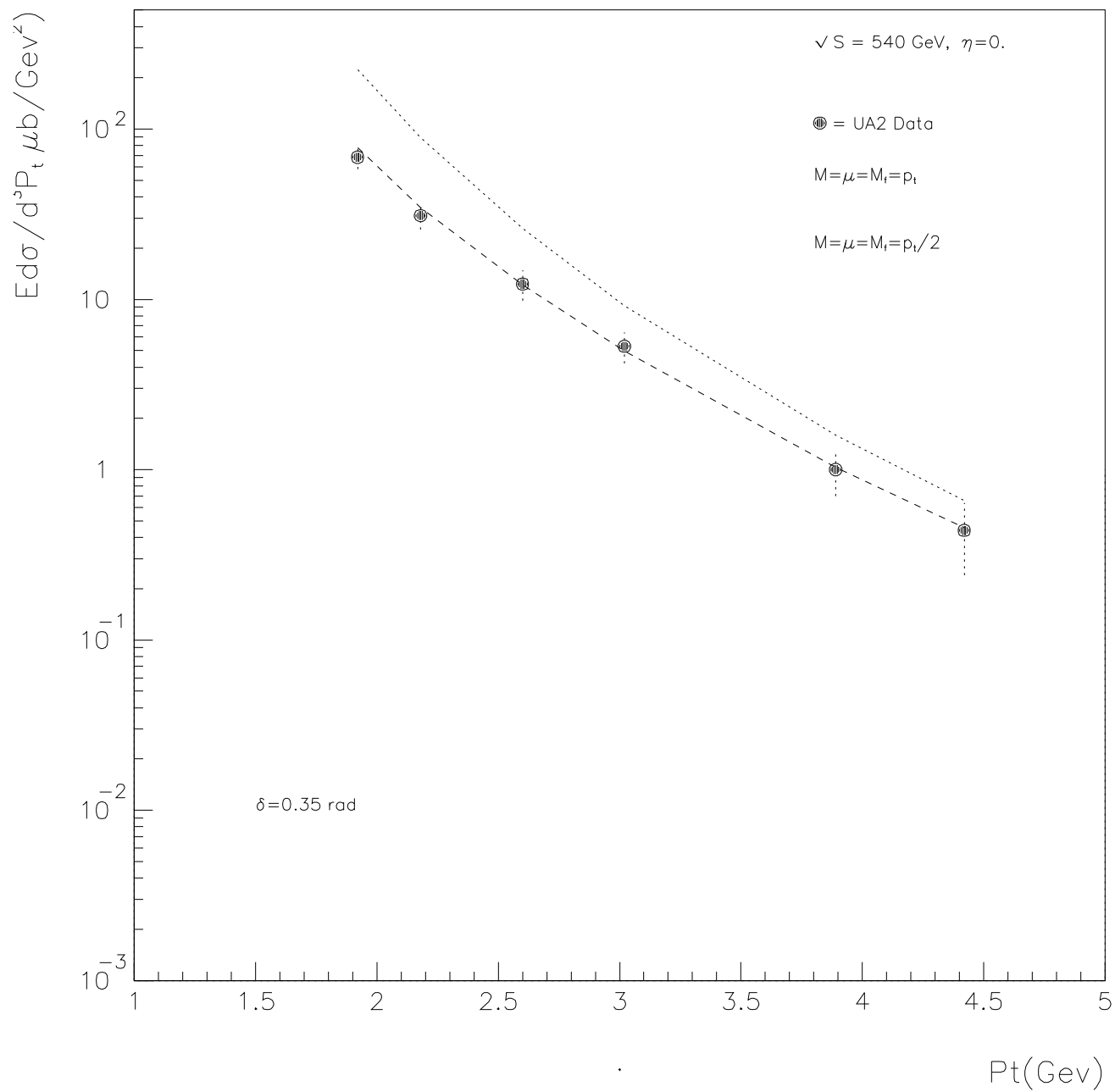


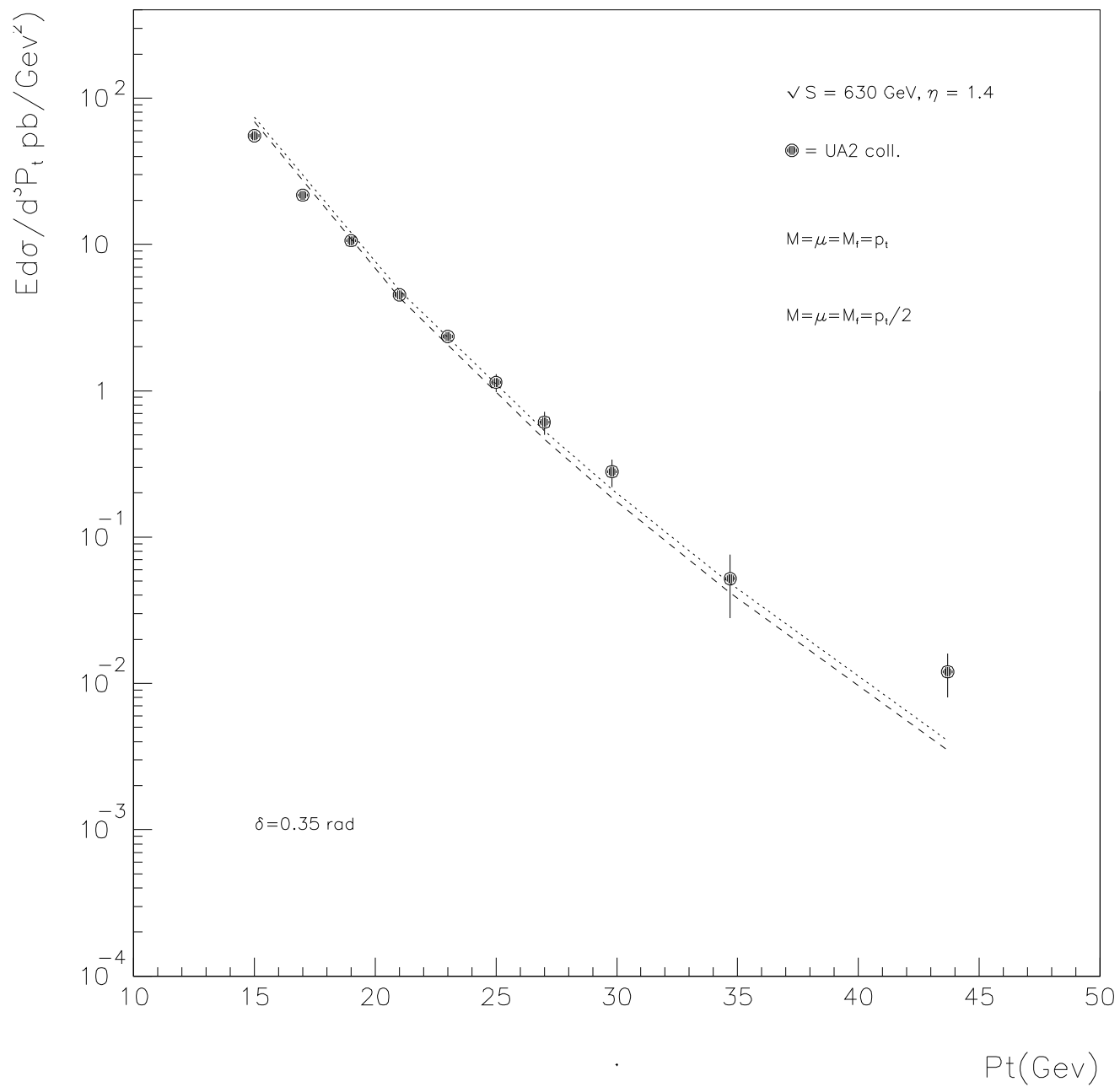


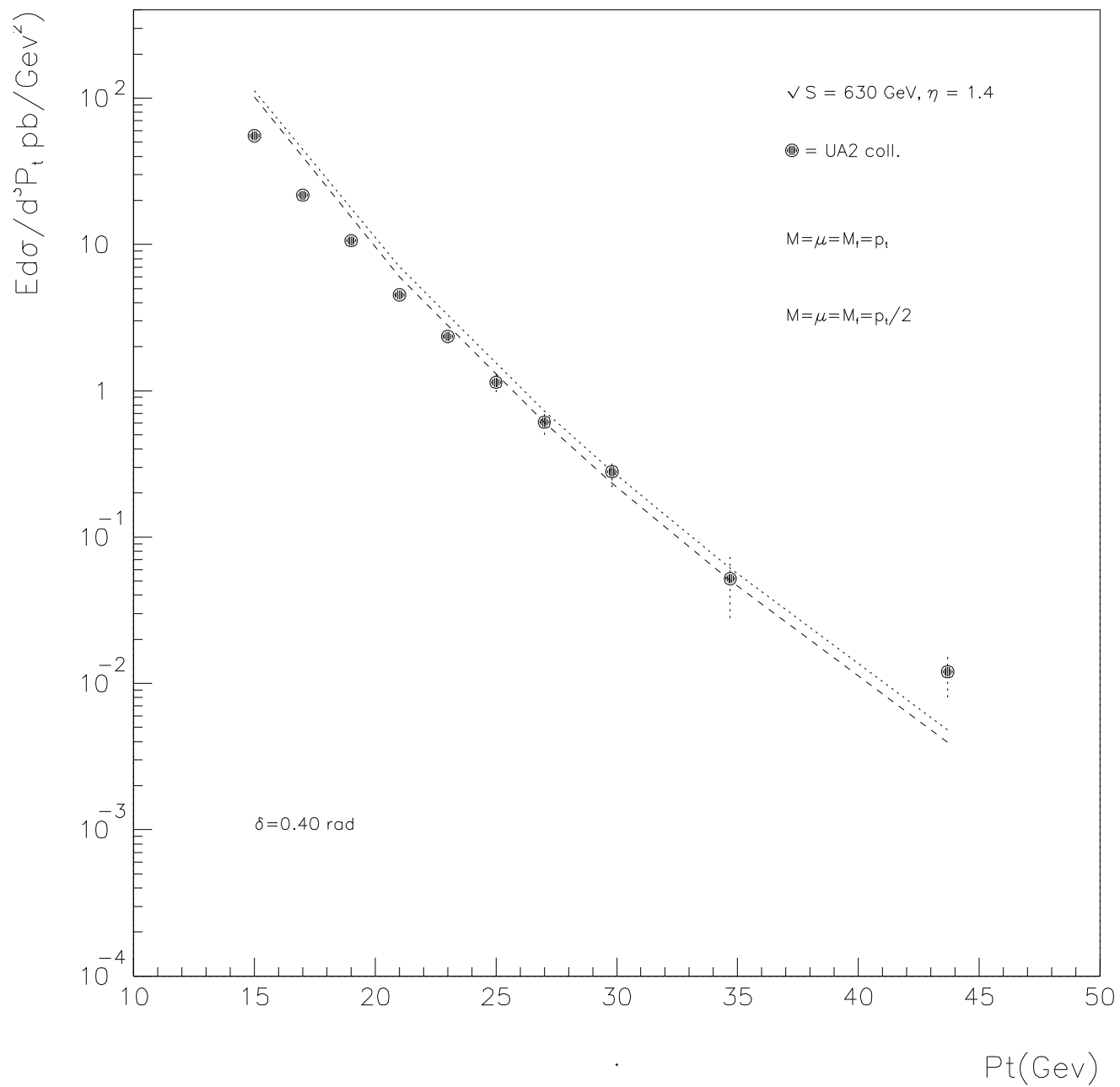




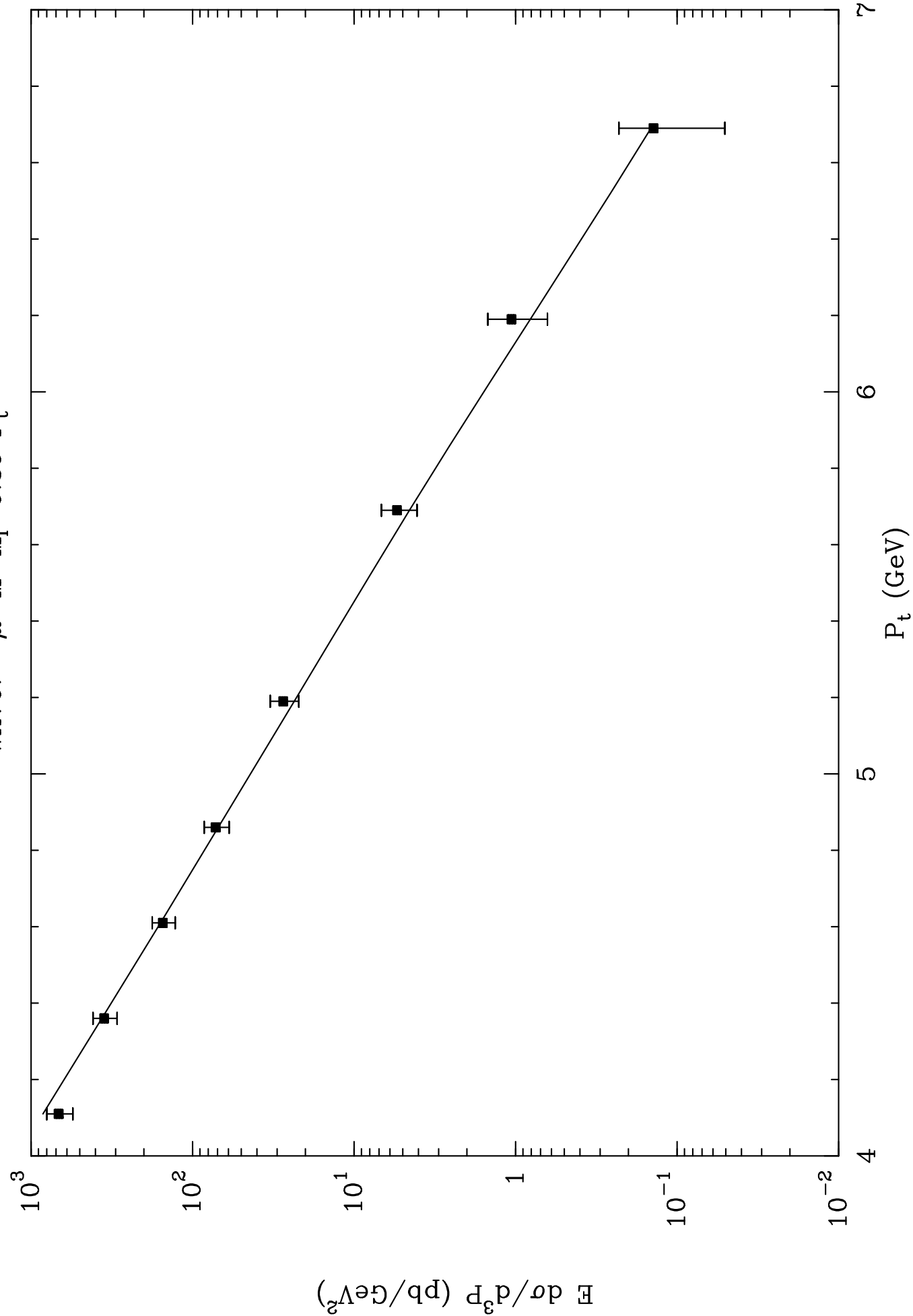




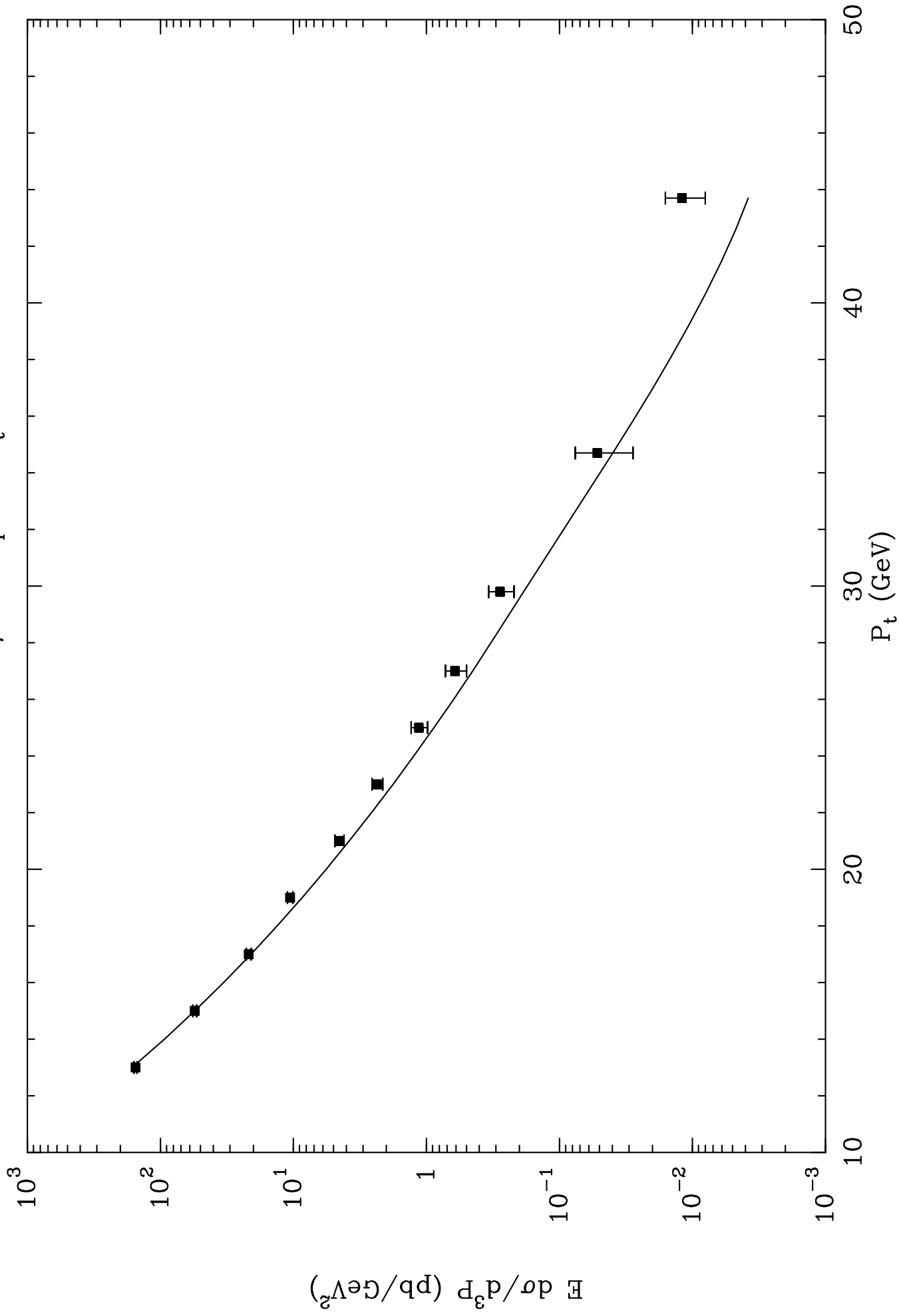




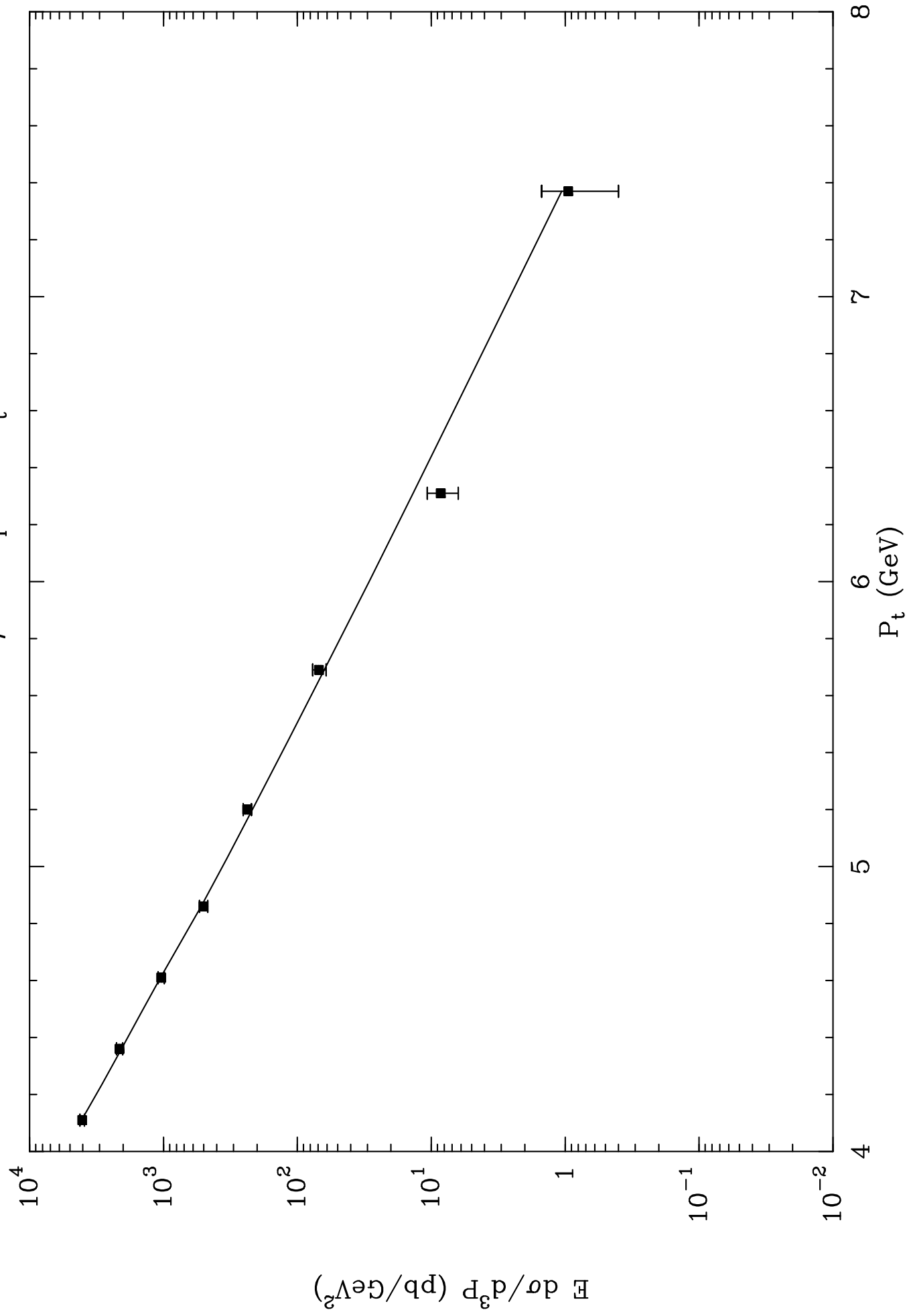
WA70: $\mu=M=M_f=0.39 P_t$



UA2: $\mu=M=M_f=5.5 P_t$

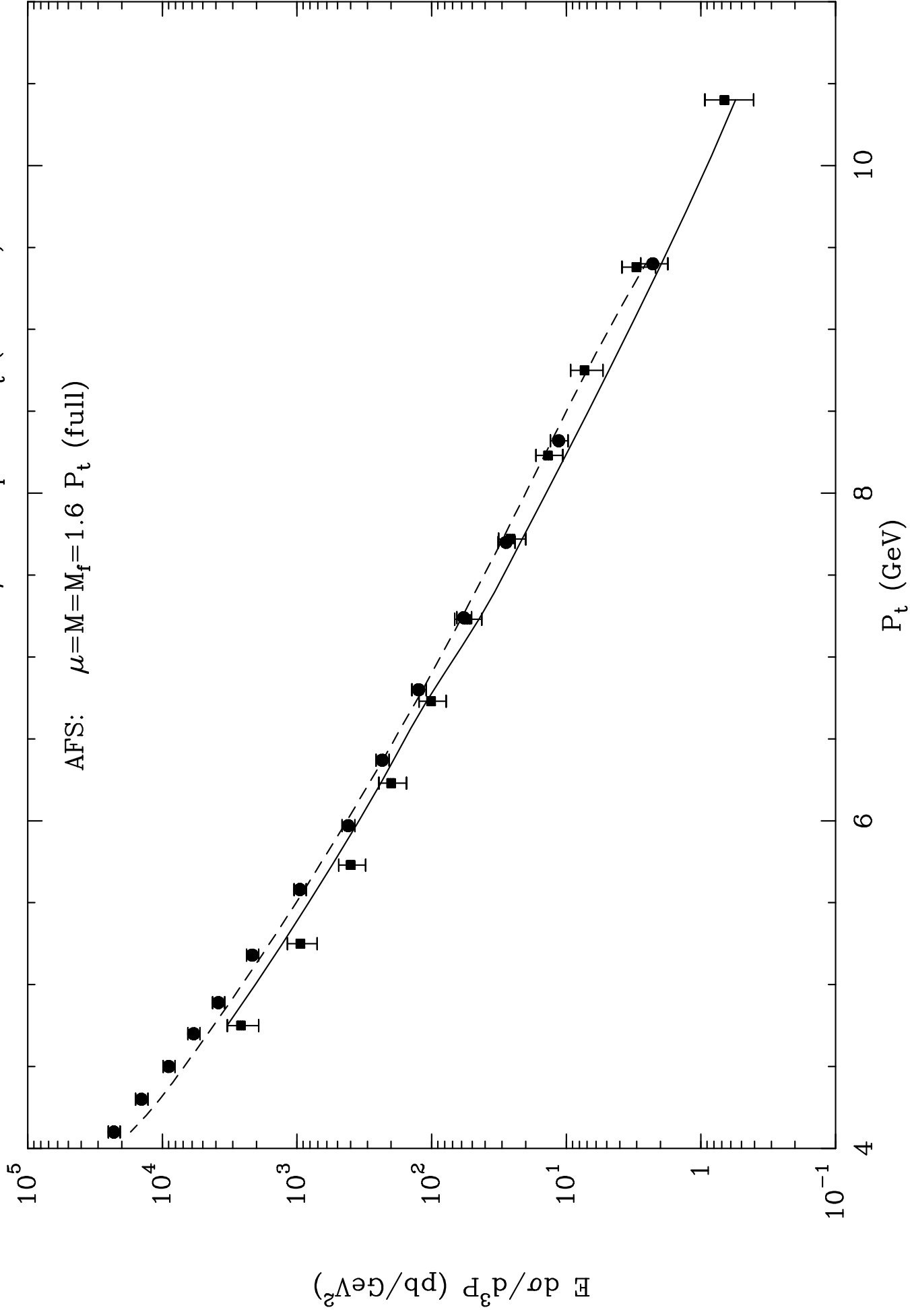


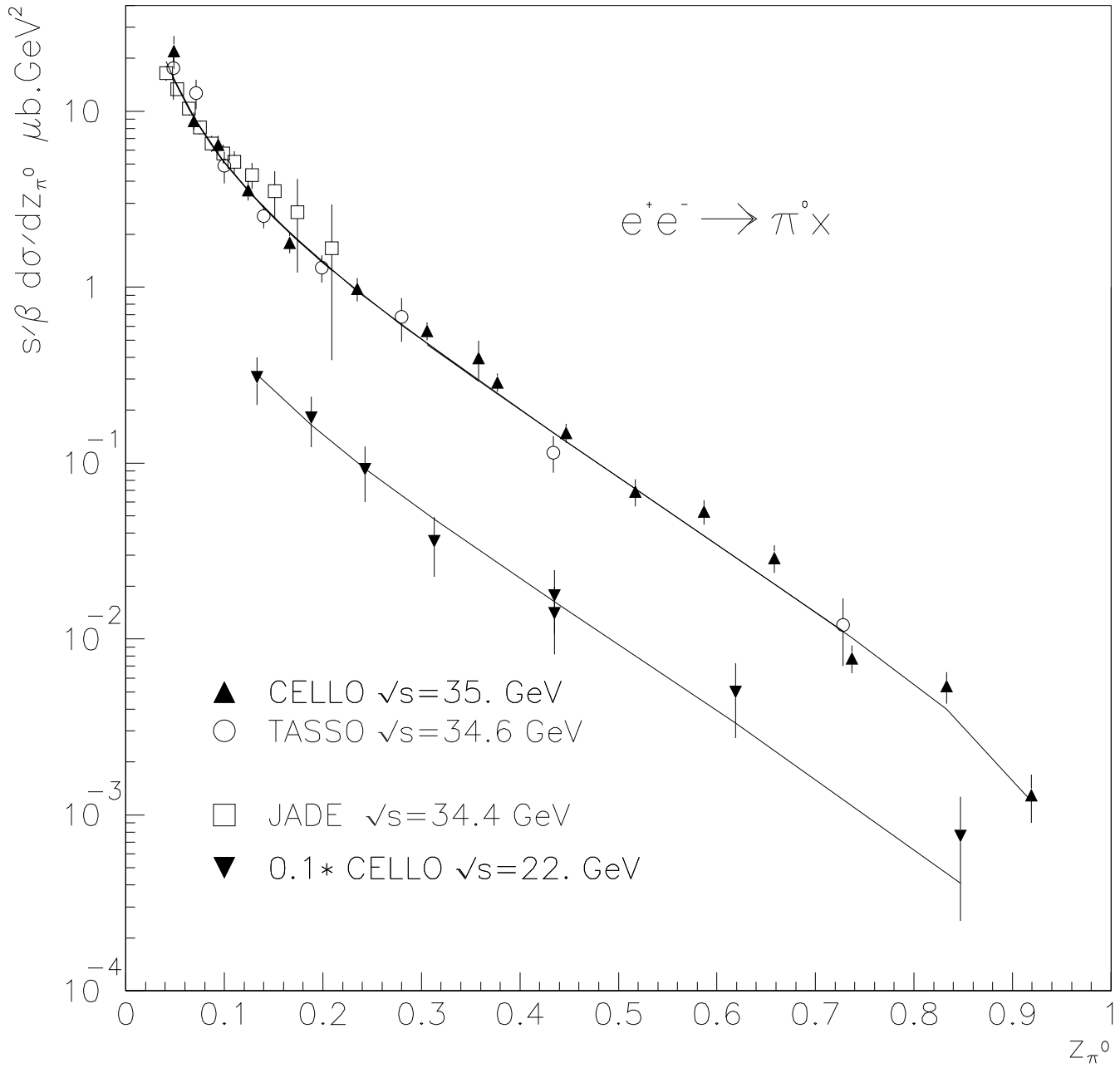
E706: $\mu=M=M_f=0.46 P_t$

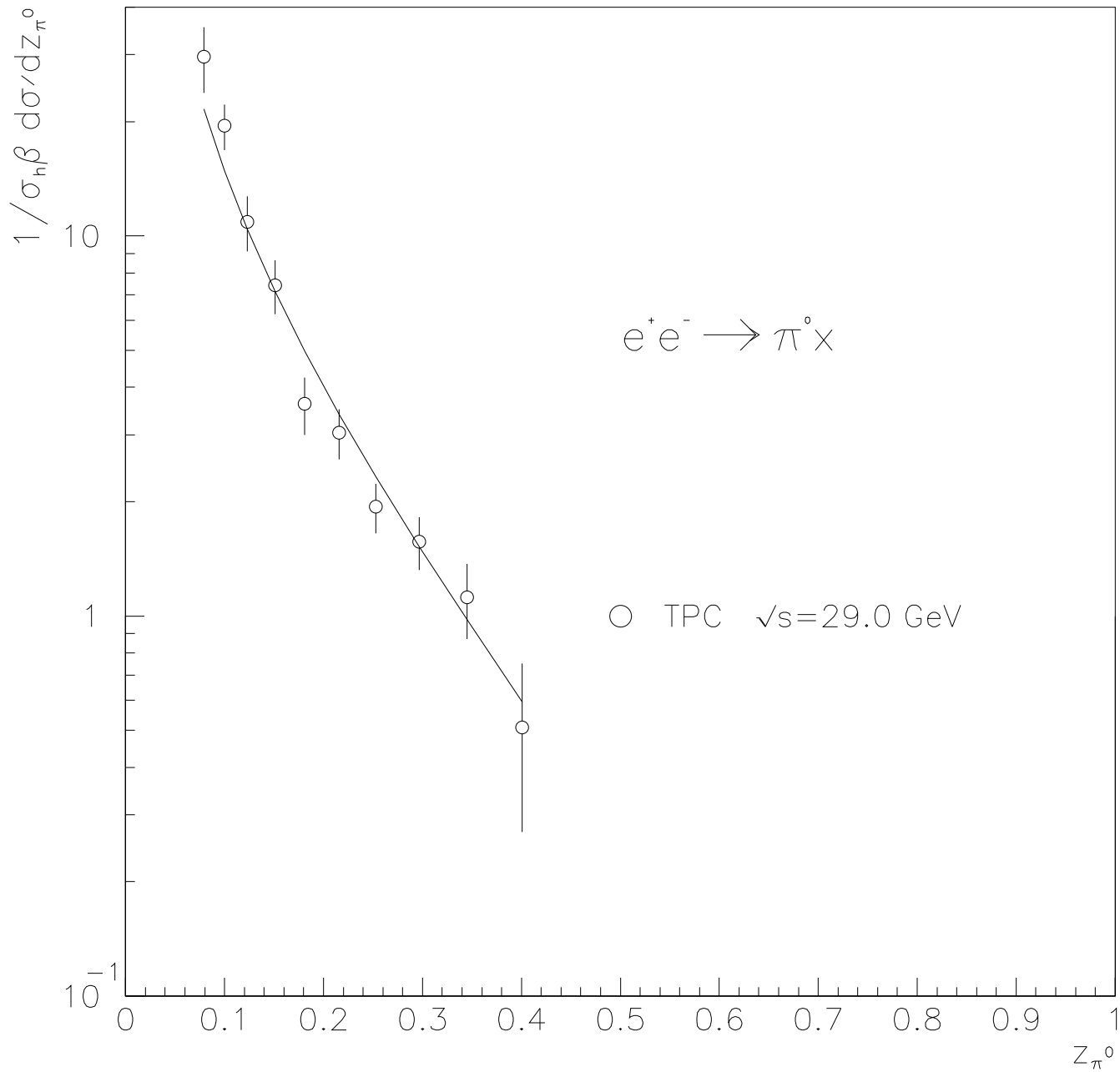


KOURKOUMELIS et al: $\mu=M=M_f=1.3 P_t$ (dashed)

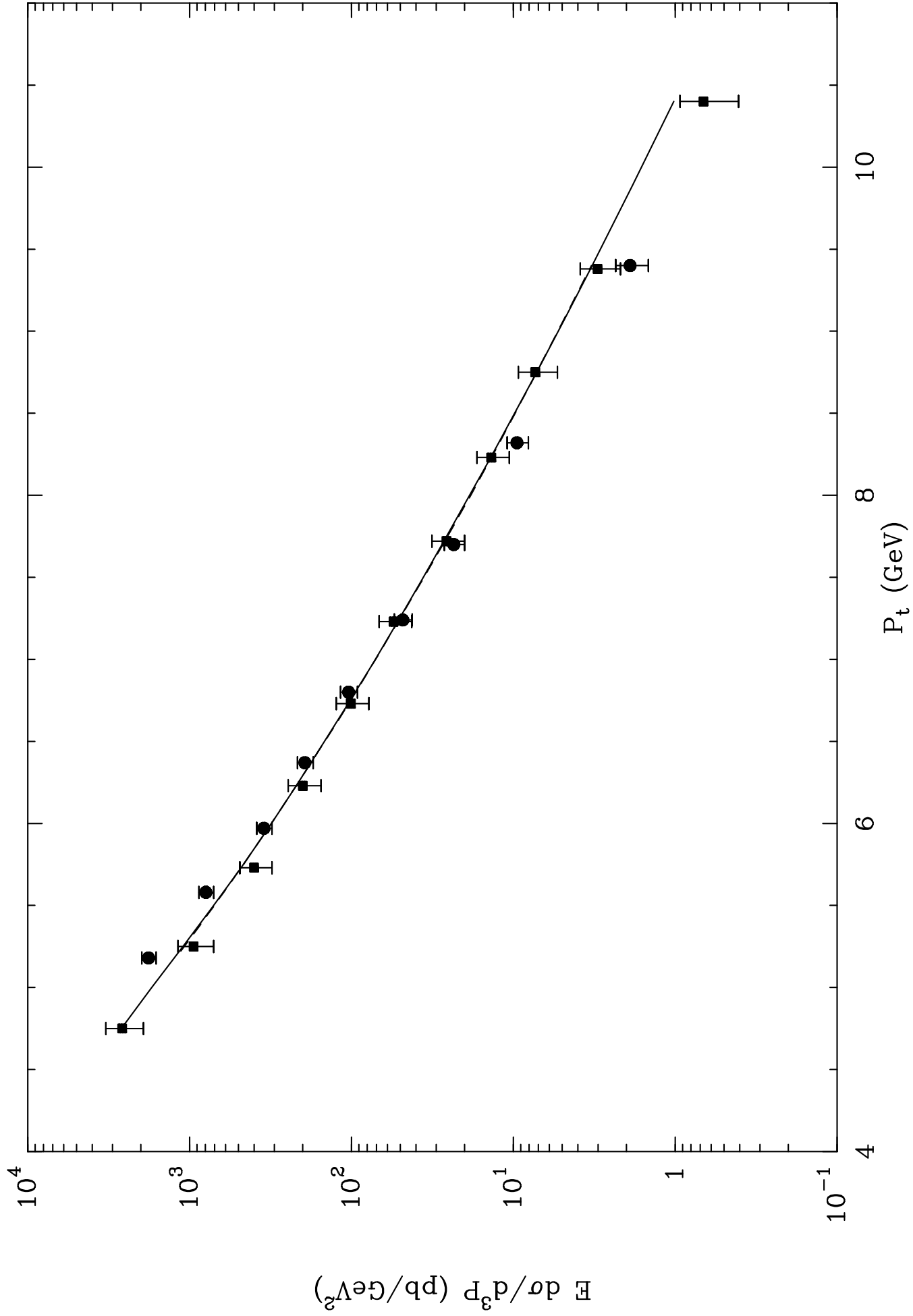
AFS: $\mu=M=M_f=1.6 P_t$ (full)



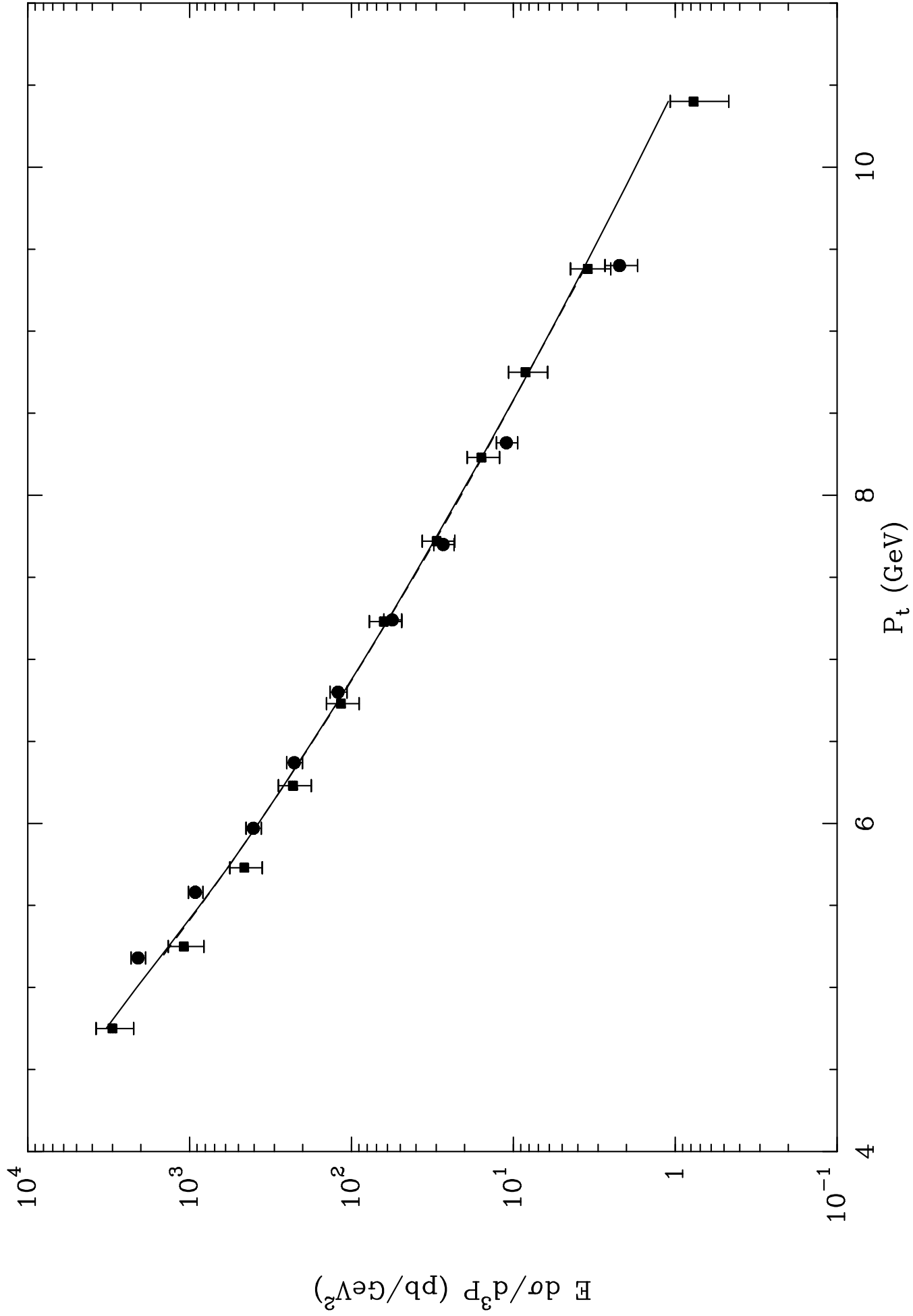




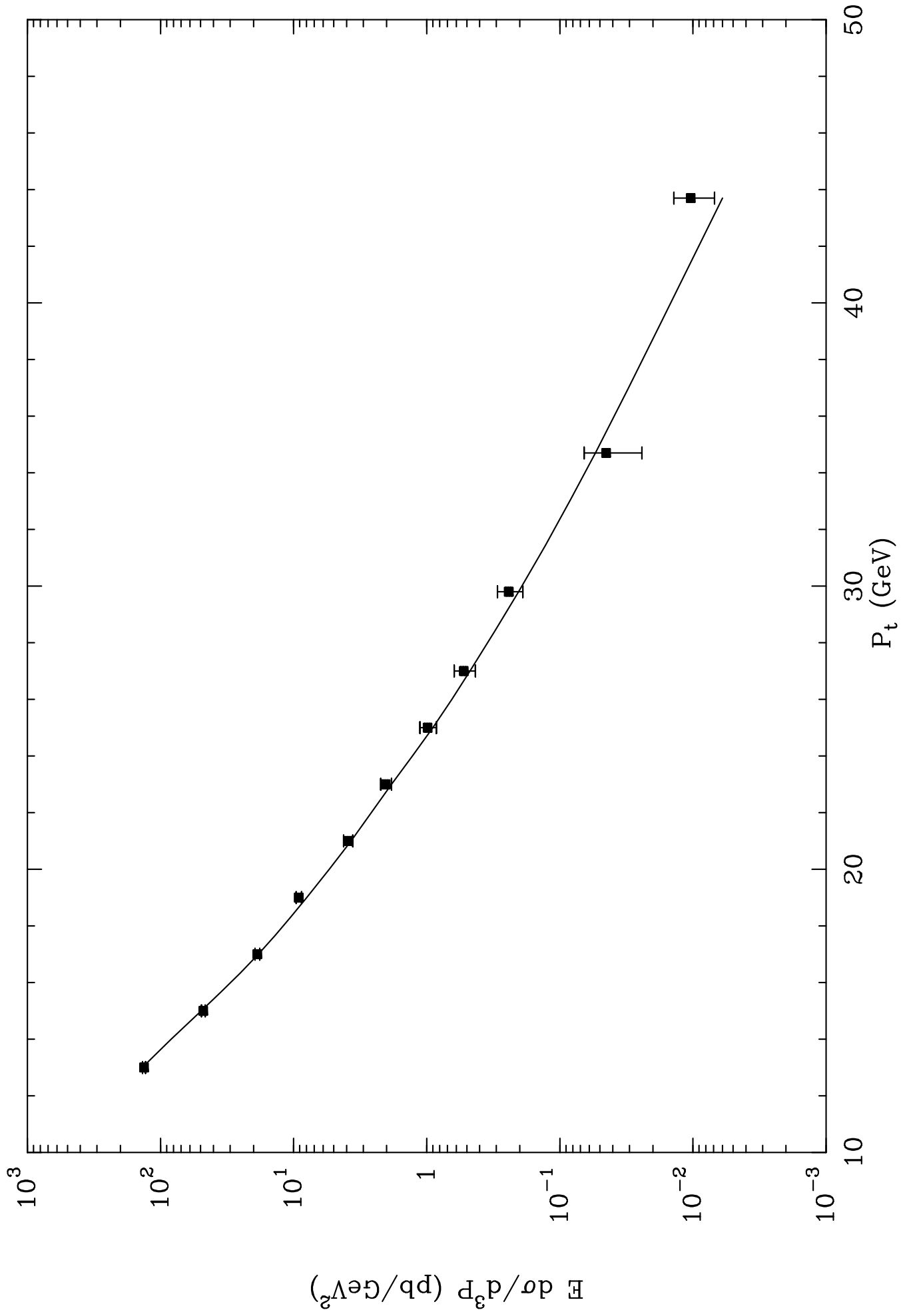
ISR: SET IIa OF FRAGMENTATION FUNCTIONS



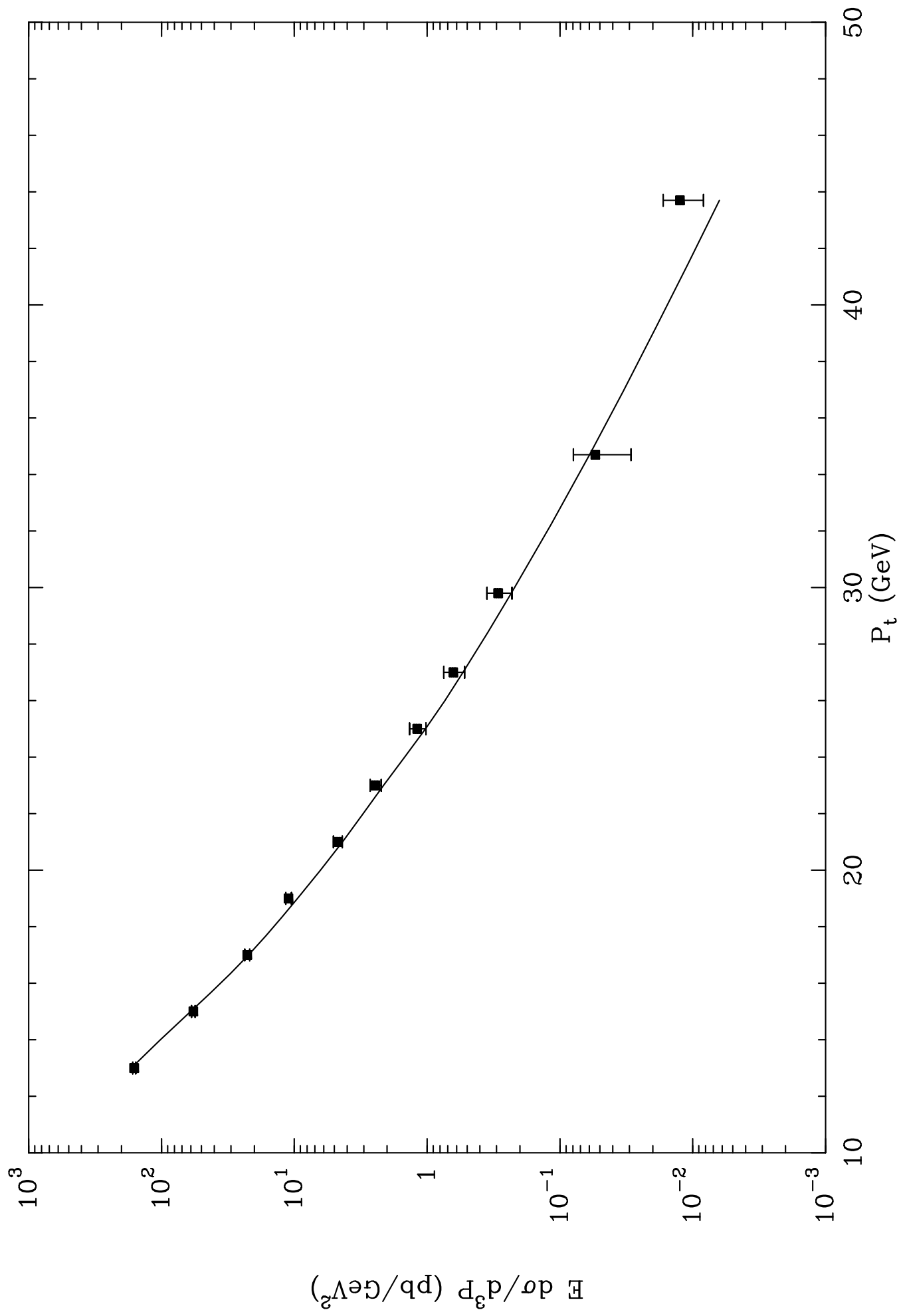
ISR: SET IIb OF FRAGMENTATION FUNCTIONS



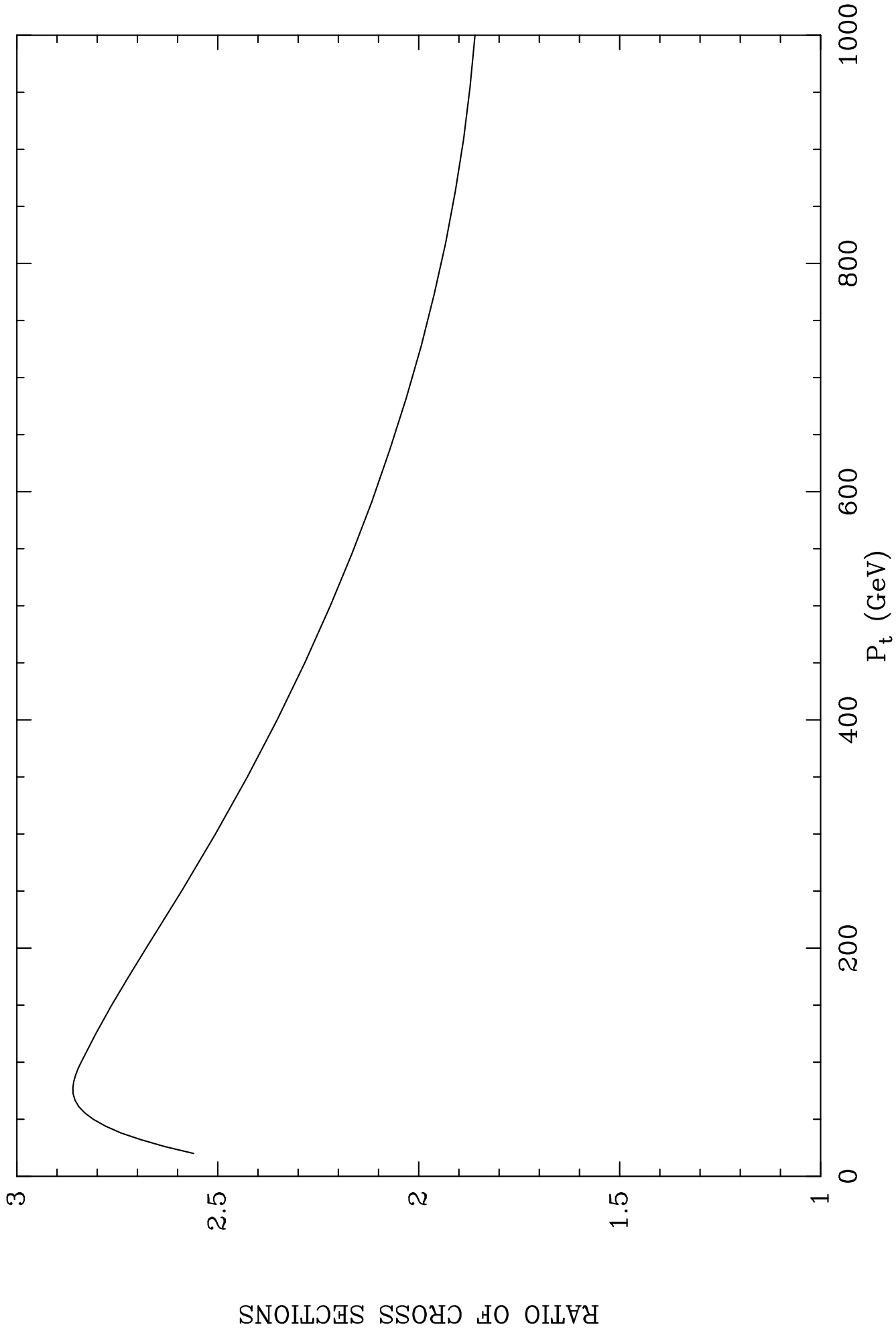
UA2: SET IIa OF FRAGMENTATION FUNCTIONS



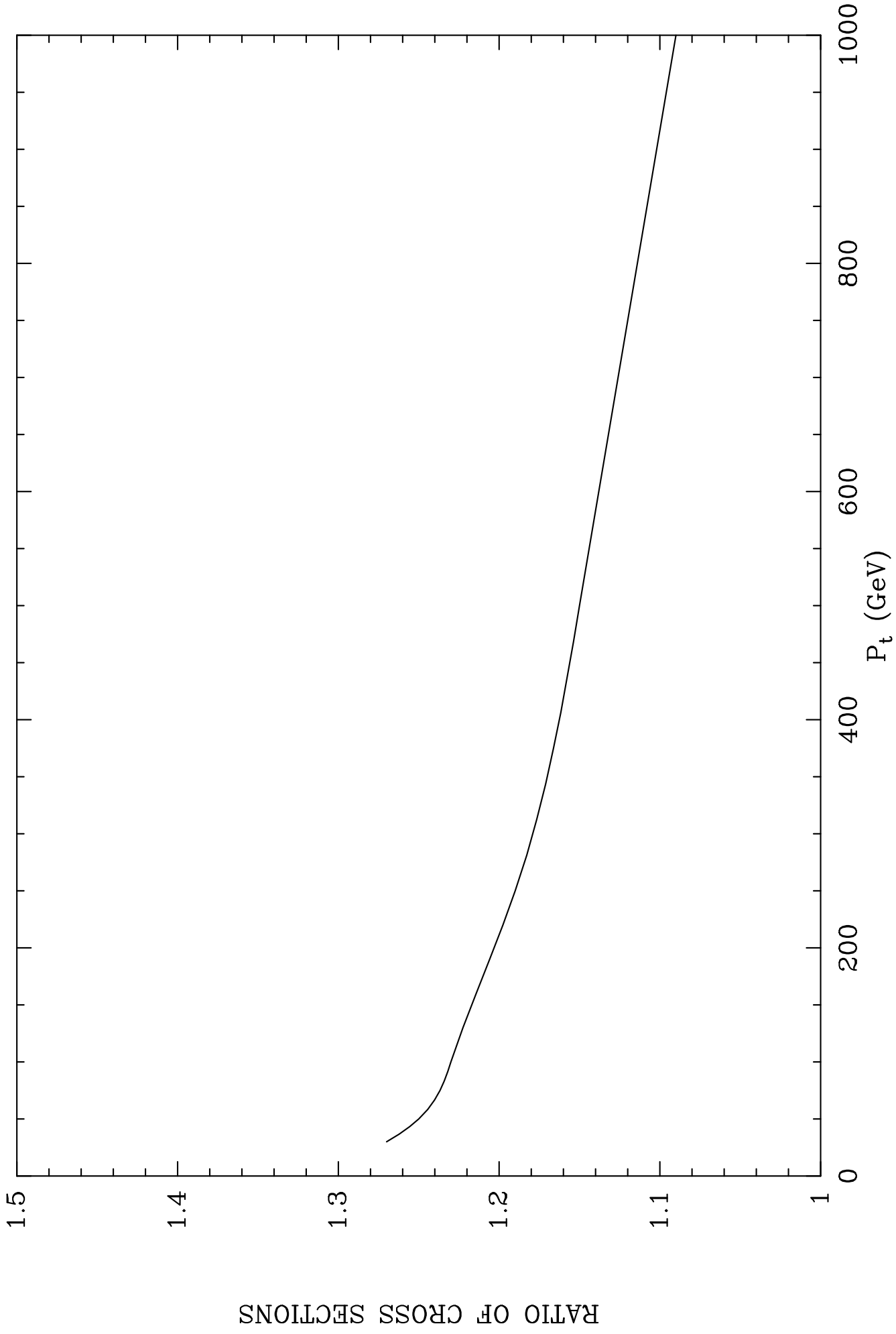
UA2: SET IIb OF FRAGMENTATION FUNCTIONS



LHC: SET I

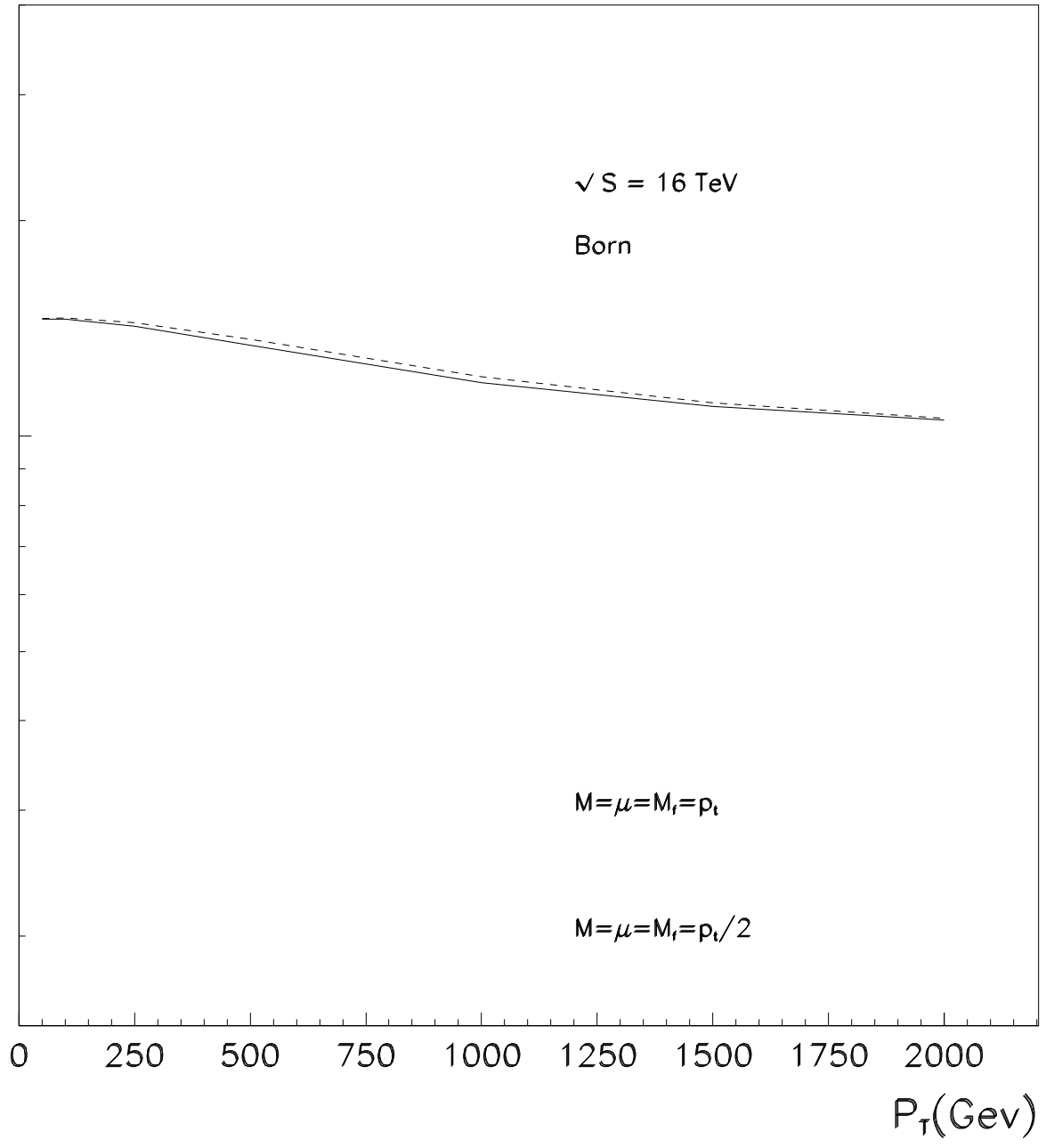


LHC: SET II



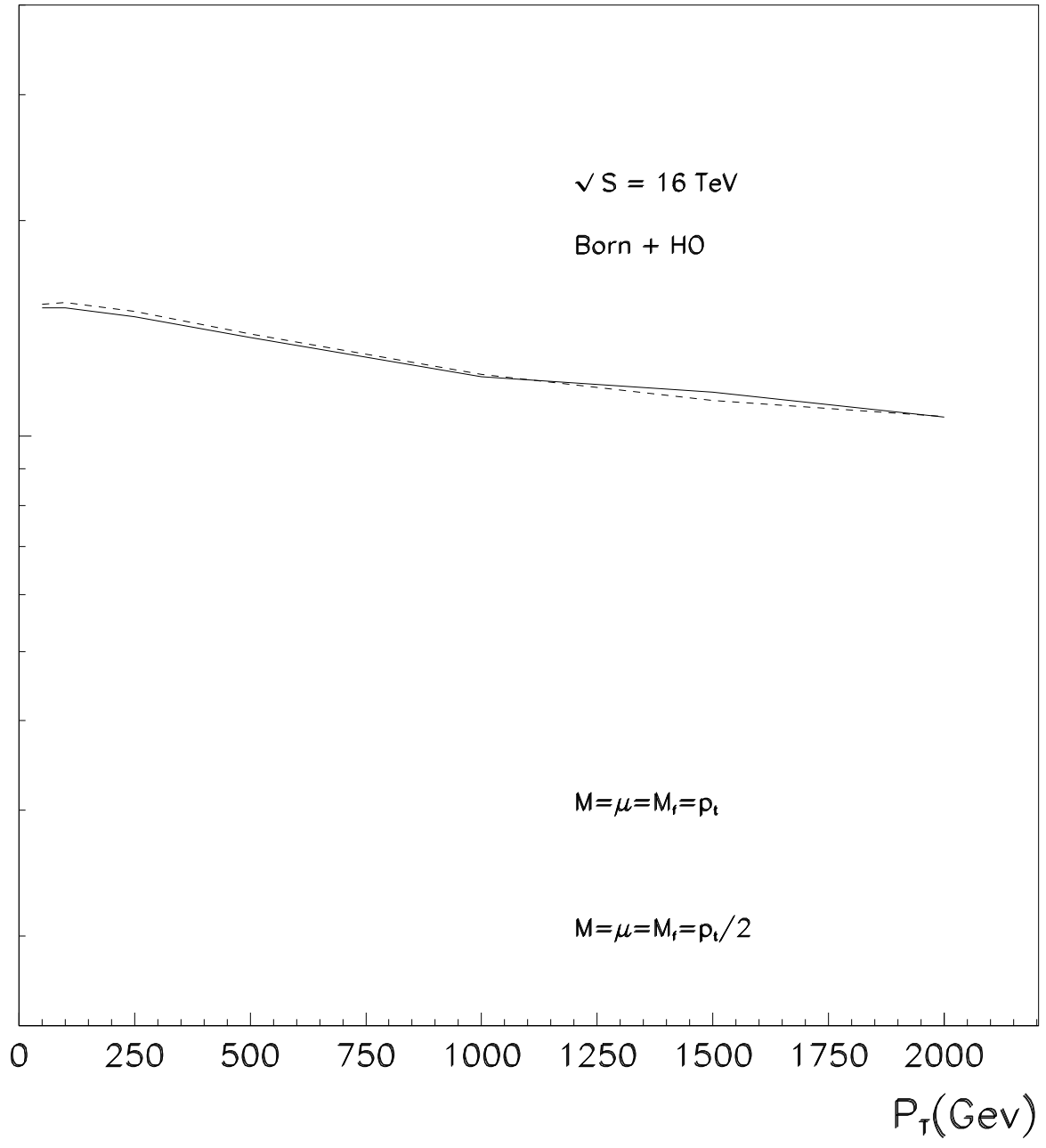
$$R = \text{Ed}\sigma / d^3P(\delta=0.4) / \text{Ed}\sigma / d^3P(\delta=0.35)$$

1

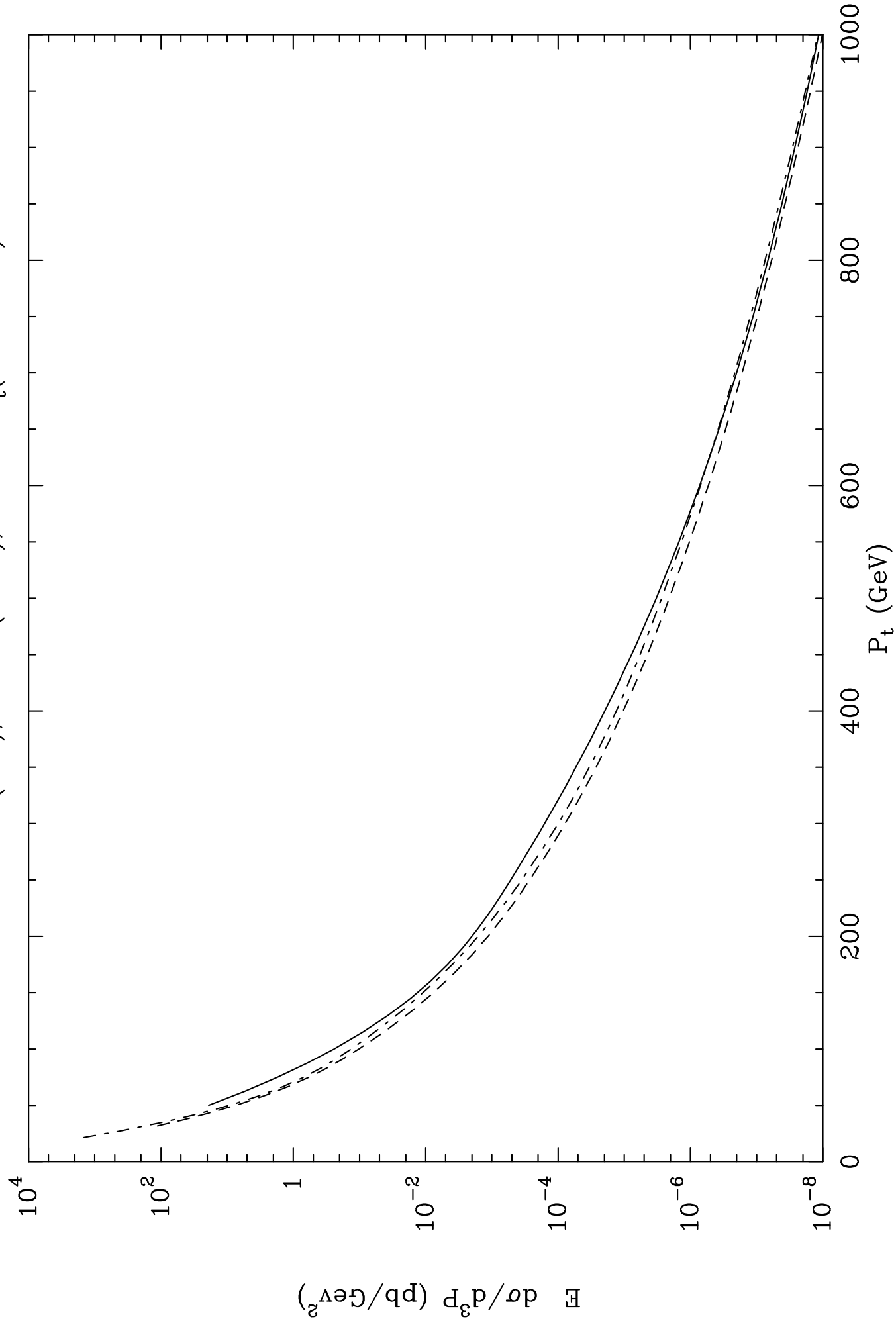


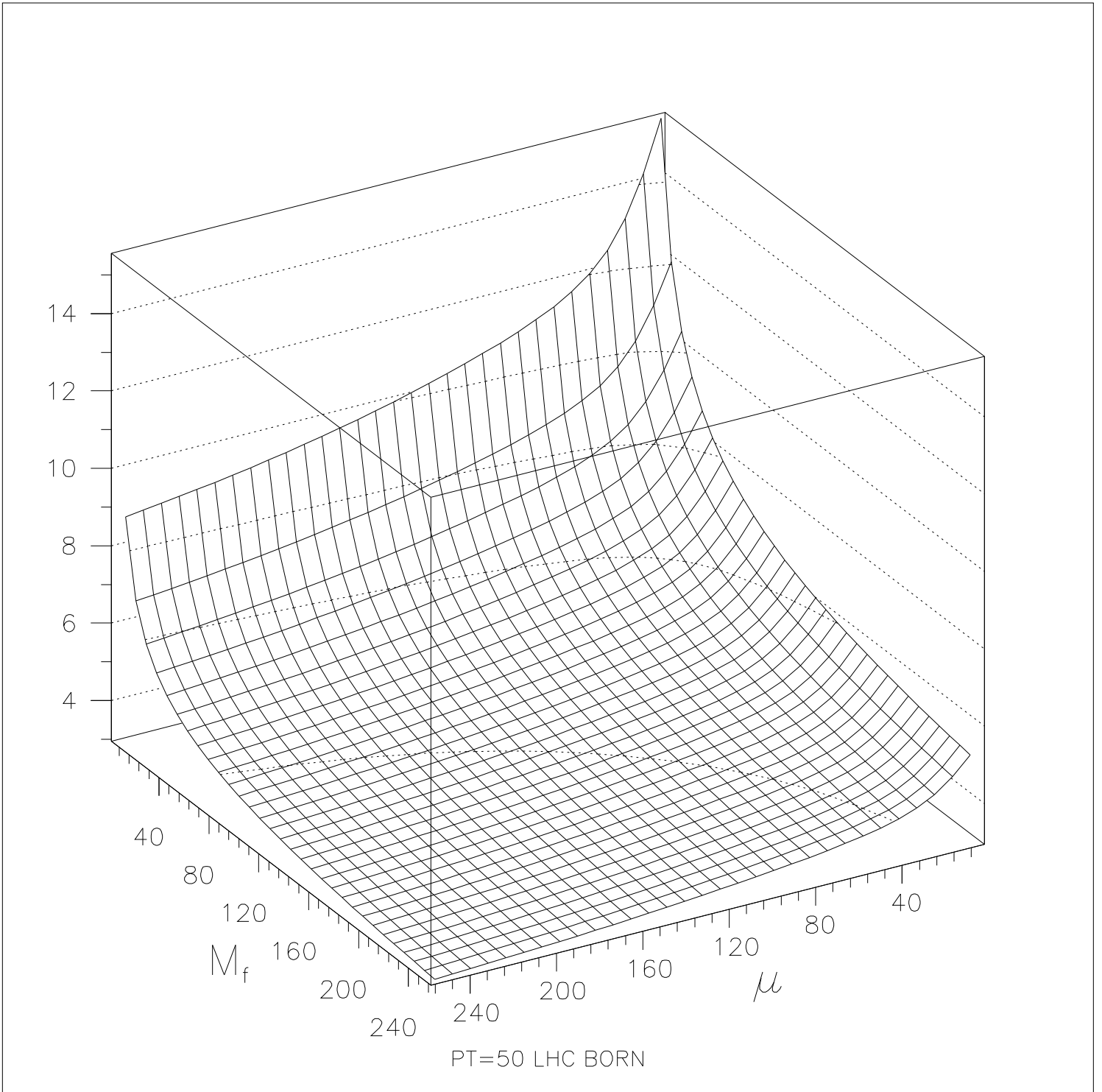
$$R = \text{Ed}\sigma / d^3P(\delta=0.4) / \text{Ed}\sigma / d^3P(\delta=0.35)$$

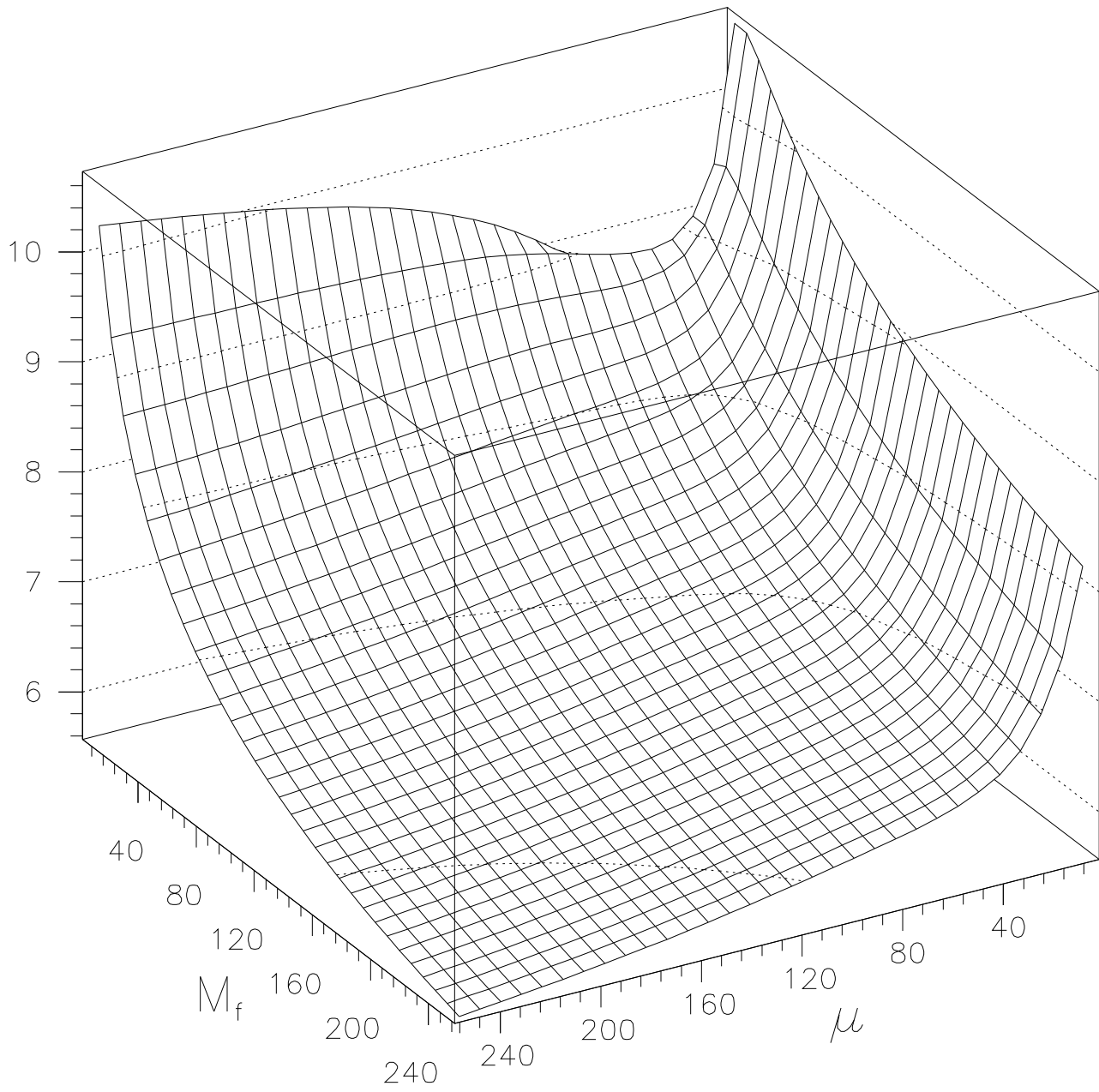
1



LHC:HERWIG(full),SET IIb(dash),SET I 50P_t(dot-dash)







PT=50 LHC B+HO

